Charles University in Prague

Faculty of Science

Study programme: Chemistry
Study branch: Biophysical chemistry

Bc. Tereza Halamová

Synthesis and characterization of new insulin derivatives with altered selectivity for insulin and IGF-1 receptors

Příprava a charakterizace nových derivátu insulinu s pozměněnou selektivitou vůči receptorům insulinu a IGF-1

Diploma thesis

Supervisor: RNDr. Jiří Jiráček, CSc.

Prague 2018

Prohlášení

Prohlašuji, že jsem tuto diplomovou práci sepsala samostatně pod vedením školitele RNDr. Jiřího Jiráčka, CSc. a všechny informační zdroje a literaturu jsem řádně citovala. Tato práce, ani její podstatná část nebyly předloženy k získání jiného nebo stejného akademického titulu.

V Praze dne: ……

Podpis: ……

Acknowledgments

I would like to thank my supervisor RNDr. Jiří Jiráček, CSc. for his patience, help and advices during my work. Also, I would like to thank RNDr. Lenka Žáková, Ph.D. and Mgr. Irena Selicharová, Dr. for helping me with binding assays and immunoblotting. My thanks also belong to Mgr. Martina Chrudinová, Mgr. Kateřina Macháčková, Bc. Kateřina Hanková and Marek Polák for always helping me out and also all of the team of Dr. Jiráček for making a friendly atmosphere.

Lastly, I would like to thank my family and my boyfriend for supporting me during my studies.

Abstrakt

Receptor insulinu (IR) existuje ve dvou izoformách (IR-A a IR-B) lišících se tkáňovou distribucí a možná i funkcí, tzn. jejich odpovědí na vazbu insulinu. Předpokládá se, že zatímco IR-A spouští zejména mitogenní procesy vedoucí k dělení a proliferaci buněk, IR-B spouští především metabolické procesy vedoucí zejména ke vstupu molekul glukosy z krve do nitra svalových a tukových buněk. Insulin se může slaběji vázat i na receptor pro růstový faktor IGF-1 (IGF-1R), který je zodpovědný hlavně za procesy spojené s vývojem a růstem organismu. Deriváty insulinu vážící se selektivně pouze na jeden z receptorů by měly velký význam pro studium receptorů, ale potenciálně i pro léčbu nemocí jako je cukrovka nebo rakovina. V této práci jsme využili zkušeností ve studiu struktury a aktivity insulinu pro návrh, přípravu a biologickou charakterizaci 4 nových derivátů insulinu s cílem pozměnit selektivitu vůči jednotlivým receptorům. Modifikace v nových analozích spočívaly v amidaci C-konce řetězce B insulinu a postupném prodlužování tohoto řetězce o 1-3 glyciny s amidovaným C-koncem. Pro všechny nové analogy byly určeny jejich vazebné afinity vůči IR-A a IR-B a pro některé z analogů i vůči IGF-1R. Nakonec byly určeny schopnosti analogů aktivovat IR-A a IR-B, tzn. indukovat autofosforylaci vnitrobuněčných podjednotek těchto receptorů. Studie přinesla informace o vlivu prodlužování C-konce B-řetězce na vazebnou specifitu insulinu vůči isoformám jeho receptoru. Analog s Gly-NH_2 v pozici B31 vykazoval více než 3x vyšší vazebnou afinitu vůči IR-B než vůči IR-A. Informace získané v této studii by mohly v budoucnu přispět k vývoji látek prospěšných pro léčbu diabetu.

Abstract

Insulin receptor (IR) exists in two isoforms (IR-A and IR-B), which differ in the tissue distribution and probably also in their function, i.e. in their response to insulin binding. It is supposed that IR-A activates mainly mitogenic processes and that IR-B triggers mainly metabolic effects resulting in the uptake of glucose by muscle and fat cells. Insulin can also weakly bind to the receptor for IGF-1 (IGF-1R), a growth factor involved in the regulation of growth and development. Insulin derivatives selectively binding only to one of the receptors would be interesting for the study of the receptors but also potentially for the treatment of diseases such as diabetes or cancer. Here we used our experience in the structure-activity studies of insulin for the design, synthesis and biological characterization of 4 new insulin derivatives in order to modify their selectivity towards the individual receptors. We systematically modified insulin by amidation of the C-terminus of its B-chain or by prolongation of the B-chain by 1-3 carboxyamidated glycine residues. Binding affinities of all new analogues for IR-A and IR-B were determined and for some of the analogues binding affinities for IGF-1R as well. Finally, abilities of analogues to activate autophosphorylation of intracellular subunits of IR-A and IR-B were determined. The study provided new information about the role of prolongation of the B-chain on the receptor binding specificity of resulting analogues. Insulin analogue with Gly-NH_2 at the position B31 of insulin had more than 3-times higher binding specificity for IR-B than for IR-A. Information obtained in this study could be useful for a development of new insulin analogues useful for treatment of diabetes.

Content

List of abbreviations

4-MePip – 4-Methylpiperidine

ACN – acetonitrile

Akt – proteinkinase B

APS – ammonium persulfate

AS160 – the Akt substrate regulating GLUT-4 translocation

Boc – *tert*-butyloxycarbonyl protecting group

BSA – bovine serum albumin

CCD camera – charge coupled device camera

DBU – 1,8-Diazabicyclo(5.4.0)undec-7-ene

DCM – dichloromethane

DIC – *N,N*-diisopropylcarbodiimide

DM – diabetes mellitus

DMA – dimethylacetamide

DMEM – Dulbecco's Modified Eagle Medium

DMF – dimethylformamide

DMSO – dimethyl sulfoxide

DOI – des(B23-B30)octapeptide insulin

DODT – 3,6-dioxa-1,8-octane-dithiol

DTT – 1,4-dithiothreitol

EDTA – ethylendiaminetetraacetic acid

Erk – extracellular signal-regulated kinase

ESI – electrospray ionization

Fmoc – 9-fluorenylmethyloxycarbonyl protecting group

GLUT-2 – glucose transporter 2

GLUT-4 – glucose transporter 4

Grb 2 – growth-factor-receptor-bound protein-2

HAc – acetic acid

HEPES – 4-(2-hydroxyethyl) -1-piperazineethanesulfonic acid

HOBt – hydroxybenzotriazole

HI – human insulin

IGF-1R – insulin-like growth factor 1 receptor

IR – insulin receptor

IR-A – insulin receptor isoform A

IR-B – insulin receptor isoform B

IRS – insulin receptor substrate

IUB – International Union of Biochemistry

IUPAC –International Union of Pure and Applied Chemistry

MAPK – mitogen-activated protein kinase

NMP – *N*-methyl-2-pyrrolidone

PDK – 3-phosphoinositide-dependent kinase

PI3K – phosphatidylinositol-3-kinase

PIP3 – phosphatidylinositol-3,4,5 triphosphate

Pac – phenacyl protecting group

pAkt – phosphorylated proteinkinase B

Raf – serine/threonine-protein kinase belonging to Raf-kinase family

Ras – small GTPase - signalling protein belonging to Ras superfamily

RP-HPLC – Reverse phase-high performance liquid chromatography

RT – room temperature

SDS – sodium dodecyl sulphate

SDS-PAGE – sodium dodecyl sulphate polyacrylamide gel electrophoresis

Shc – Src-homology-2-containing protein

Solution A – 0,1%TFA in deionized water

Solution B – 80% ACN in deionized water in presence of 0,1% TFA

SOS – Son-of-sevenless

tBu – *t*-butyl protecting group

TCEP – tris(2-carboxyethyl)phosphine hydrochloride

TEMED – tetramethylethylenediamine

TFA – trifluoroacetic acid

TIS – triisopropylsilane

Trt – trityl protecting group

T-TBS – Tween-Tris-buffered saline

Furthermore, the single letter abbreviations for amino acids used according to the recommendations of IUPAC-IUB [1]. Unless otherwise stated, these are amino acids in the L-form.

1. Introduction

Diabetes mellitus is in today's world considered to be an epidemic of the 21st century. To the year 2017 it was estimated that 425 million of people worldwide suffer with diabetes [2]. This means that every 11th adult has diabetes.

Despite the fact that the treatment of diabetes with insulin analogues is well-established in clinical practice, the outcome is still sub-optimal (see below). Pursuit of "perfect insulin" is still a point of interest.

1.1. Insulin

Insulin is a small protein (51 amino acids) consisting of two chains A and B, which are connected with two disulphide bridges (Figure 1) [3].

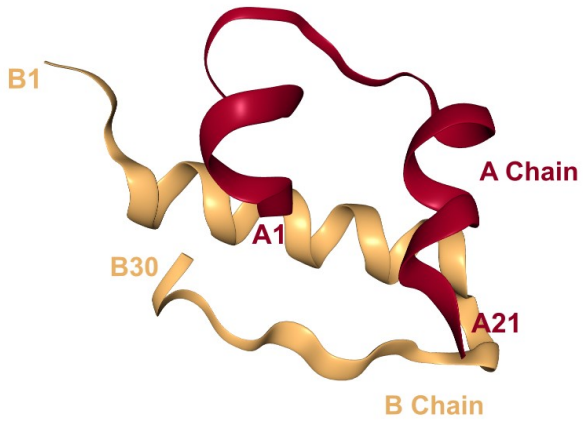

Figure 1. Crystal 3D structure of insulin. A-chain (21 residues) is in red, B-chain (30 residues) is in yellow. Disulphide bridges are not shown. Reproduced from Ref. [4].

Insulin acts as a key hormone in the blood glucose levels maintenance mechanisms. It enables glucose entrance from blood to muscle and adipose tissue, it is also responsible for regulation of liver enzymes involved in the storage of glucose in form of glycogen and in the regulation of the utilization of glucose energy [5].

Aside from its metabolic function insulin also has a growth hormone functionality. It stimulates replication of DNA and proteosynthesis. It also stimulates fat formation from blood fatty acids and it inhibits lipolysis, proteolysis and it also inhibits gluconeogenesis and glycogenolysis [5][6].

In the circulation and at low concentrations, insulin is present in a form of monomer, however at micromolar concentration it forms dimers and in the presence of zinc ions it associates into hexamers [7].

1.2. Insulin and IGF-1 receptors

Insulin binds to its receptor (IR-A and IR-B isoforms) with subnanomolar affinities and it binds with about 1000-fold lower affinity also to the receptor for IGF-1 (IGF-1R) [8]. Both IR and IGF-1R are receptor tyrosine kinases, which belong to a family of more than 60 receptors. Both receptors are homodimeric transmembrane glycoproteins consisting of 4 subunits linked by disulphide bridges (Figure 2, page 12) [9][10]. They consist of two extracellular α subunits and two partly extracellular, transmembrane and partly intracellular β subunits with tyrosine kinase activity. IR and IGF-1R share more than 50% amino acid homology overall and 84% homology in the tyrosine kinase domains [8][11].

Eleven distinct regions (domains) have been identified in each monomer of IR. Starting from the N-terminus they are: L1 (leucine rich), CR (cysteine rich), L2, FnIII-1 (fibronectin type III domain), FnIII-2a, ID (insert domain) and α-CT (C-terminal peptide) in the α subunit and ID (insert domain), FnIII-2b and FnIII-3, two regulatory transmembrane and juxtamembrane domains and intracellular tyrosine kinase catalytic domain in the β subunit (Figure 2, page 12) [9][10].

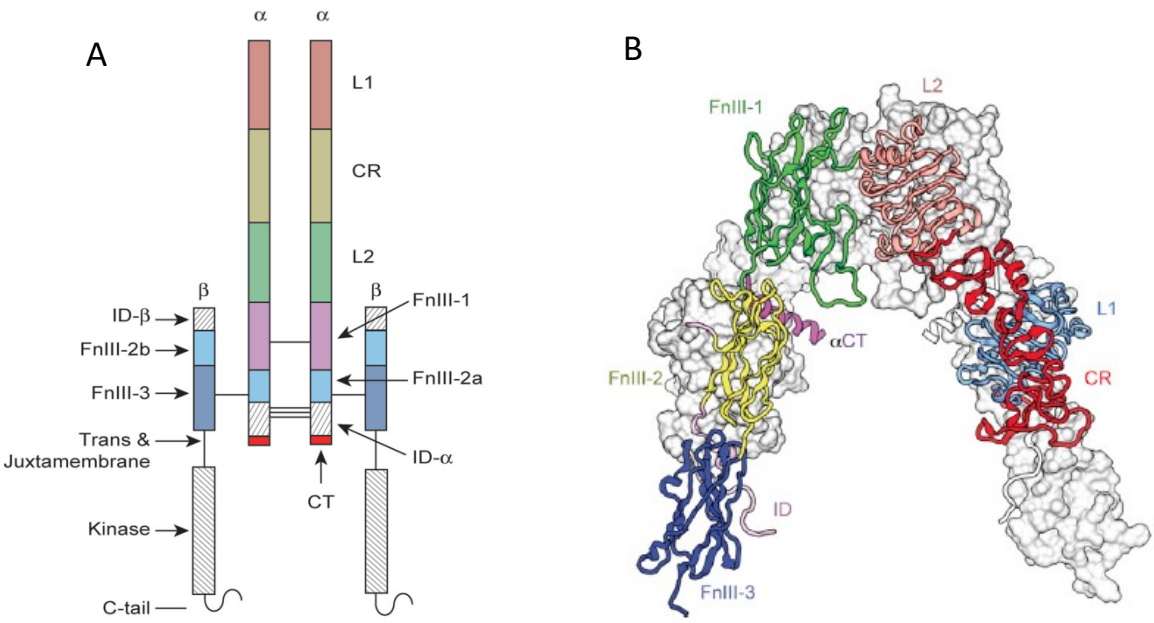

Figure 2. A. Schematic diagram of IR and IGF-1R $(\alpha\beta)_2$ homodimer. Reproduced from Ref. [12]. B. The insulin receptor (isoform A) extracellular ectodomains forming V-shaped dimeric structure. One of the monomers is coloured to show L1 (light-blue), CR (red), L2 (light-pink/salmon), FnIII-1 (green), FnIII-2 (yellow), FnIII-3 (dark-blue) domains. Also, so called α-CT segment, where the difference of two isoforms of IR occurs, is highlighted on 2A (red) and on 2B (pink). The second monomer is shown in grey as an electron surface. Reproduced from Ref. [13].

Crystal or any other structure of the whole transmembrane IR has not been solved yet for any receptor of the tyrosine kinase family.

IR exists in two isoforms, IR-A and IR-B, which differ in presence (IR-B) or absence (IR-A) of twelve amino acids at the C-terminus of the α subunit. This leads to longer or shorter so-called α-C-terminal (α-CT) segment of the receptor (in red in Figure 2A). The presence of this short sequence is encoded by exon 11 [14].

IR isoforms also have different tissue distribution in the body. Whereas IR-A is mainly expressed in the brain, spleen, lymphatic tissue and foetal tissue, IR-B is dominant in the liver (95%), heart, skeletal muscle and subcutaneous fat (70%). IR-A is associated with more mitogenic actions activating MAPK pathway, while IR-B with more metabolic actions of insulin activating PI3K/Akt pathway (discussed in 1.4.) [15]. Nevertheless it is not clear whether the mechanisms and connection from binding-to-action can be assigned to individual isoforms as it can be quite possibly caused more by specific ligand binding

properties (different k_{on} or k_{off}) or by a differential IR isoform tissue distribution or by different expression of intracellular signalling proteins [16].

IGF-1R receptor is mostly responsible for proliferation, protection of cells from programmed cell death, growth in foetal and postnatal development [9].

Apart from individual IR isoforms and IGF-1R, the so-called hybrid receptors, combining IR-A/B with IGF-1R, exist, where one monomer is made up of IR-A/B and second monomer of IGF-1R [17][18]. Existence of these receptor heterodimer hybrids contributes to an even more complex insulin-receptor regulation system.

1.3. Interaction of insulin with IR

The interaction of insulin with IR (and IGF-1R) is still a subject of an on-going research and its precise binding mechanism has not yet been elucidated structurally [19].

Insulin is supposed to have two distinct binding surfaces, by which it binds to the IR. The first is referred as the "classical binding surface" or "site 1" and second as the "second binding surface" or "site 2". Based on mutagenesis studies, Site 1 should include residues GlyA1, IleA2, ValA3, GluA4, TyrA19, AsnA21 GlyB8, SerB9, LeuB11, ValB12, TyrB16, PheB24, PheB25 and TyrB26 [7][20]. Site 2 should consist of residues A8Thr, IleA10, Ser A12, LeuA13, GluA17, HisB10, GluB13, and LeuB17 (Figure 3) [7][19][21][22].

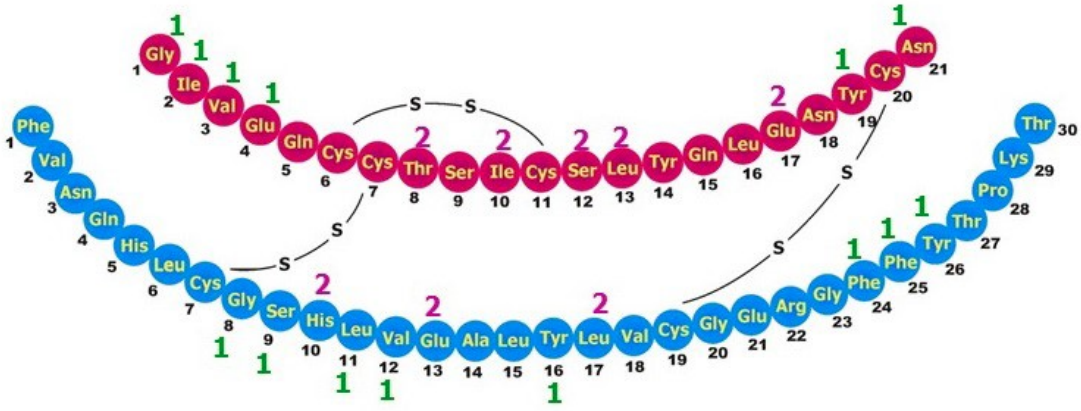

Figure 3. Primary structure of insulin. Chain A is depicted in red and chain B in blue. Site 1 residues of insulin are highlighted with green 1. Hypothetical Site 2 residues are highlighted with purple 2.

The classical binding surface of insulin consists mainly of insulin residues involved in insulin dimerization and connects insulin with IR primary binding Site 1', which was in

2013 and 2014 defined by the crystal structures of the first complex of insulin and IR fragment. It comprises of α-CT peptide of one monomer and L1 of the opposite monomer of the IR [23][24]. In this interaction the C terminus of B chain of insulin has to undergo a transition, in which it detaches from the centre of the molecule in about 60 degrees [24]. This leads to insertion of C terminus of the B chain between L1 domain and αCT peptide without steric clash (Figure 4). An alternative view of the interaction of insulin with the Site 1 of IR-A is shown in Figure 5 (page 15).

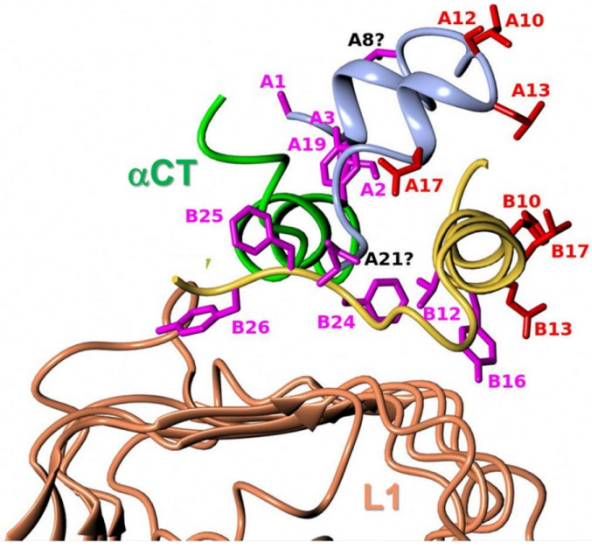

Figure 4. Crystal structure of insulin sitting on the Site 1' of IR-A. A chain of insulin depicted in blue, B chain in yellow. L1 domain of IR in beige, αCT segment in green. The residues of insulin Site 1 are represented in purple and anticipated residues of insulin Site 2 are in red colour. Reproduced from Ref. [19].

The second binding site of insulin should mostly consist of insulin residues involved in hexamerization of insulin and should interact with IR Site 2', its identity was elusive until recently [25] and it was supposed that IR Site 2' presumably lays at the junction of FnIII-1 and FnIII-2 domains (in position opposite to L1 site 1) (Figure 2B, page 12 and Figure 4). The first structural insight into the second binding surface of insulin and IR was published only few weeks ago [26]. The Cryo-EM structure of extracellular ectodomain of IR confirmed crystallographic data about Site 1' and proposed that Site 2 in insulin is formed only by residues CysA7, ThrA8 and B-chain residues B4-B10 (Figure 5, page 15) and by residues 495-498, 539-541 and 575 in IR FnIII-1 domain. This result was surprising because especially the extent of Site 2 in insulin is much more limited than predicted by mutagenesis (see above). It is not ruled out, that some new future discoveries will correct these findings.

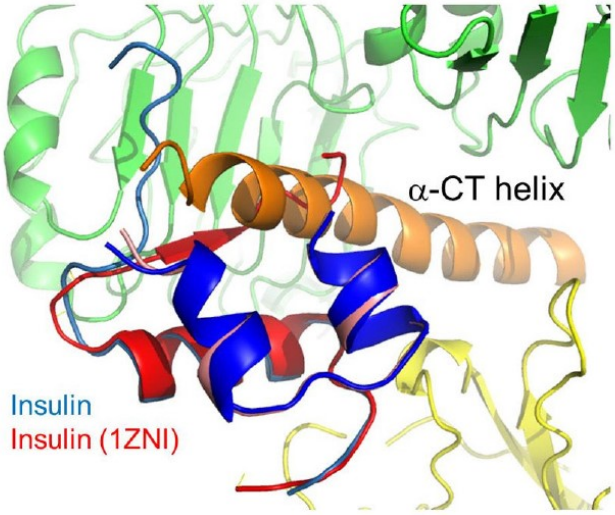

Figure 5. CryoEM structure of the complex of insulin and insulin receptor. Bound insulin is in blue and is overlaid with free insulin in red (PDB1ZNI). Site 1' of the receptor is represented by L1 in green and α-CT peptide in orange. Site 2' of the receptor is in yellow and belongs to FnIII-1 domain. Reproduced from Ref. [26].

All available structures of the complexes of bound insulin and the receptor (Figures 4 and 5) contain only a short, IR-A, version of α-CT peptide. Therefore, the position of extra 12 C-terminal amino acids of IR-B is unknown. However, it is not excluded, that they could interact with the C-terminus of the B-chain of insulin as both C-termini (of the B-chain of insulin and of the α-CT) are in the available complexes in a relative proximity (Figure 6, page 16) [27]. In a publication from 2016 [28], J. Jiráček's team showed, that the prolongation of the C-terminus of the B-chain of insulin by one to four amino acids can lead to preferential IR-B activation. Hence, it is possible that α-CT peptide points in the same direction as the end of the C-terminus of B chain and that the prolongation of the C-terminus of the B-chain could lead to some favourable interactions with longer αCT segment of IR-B.

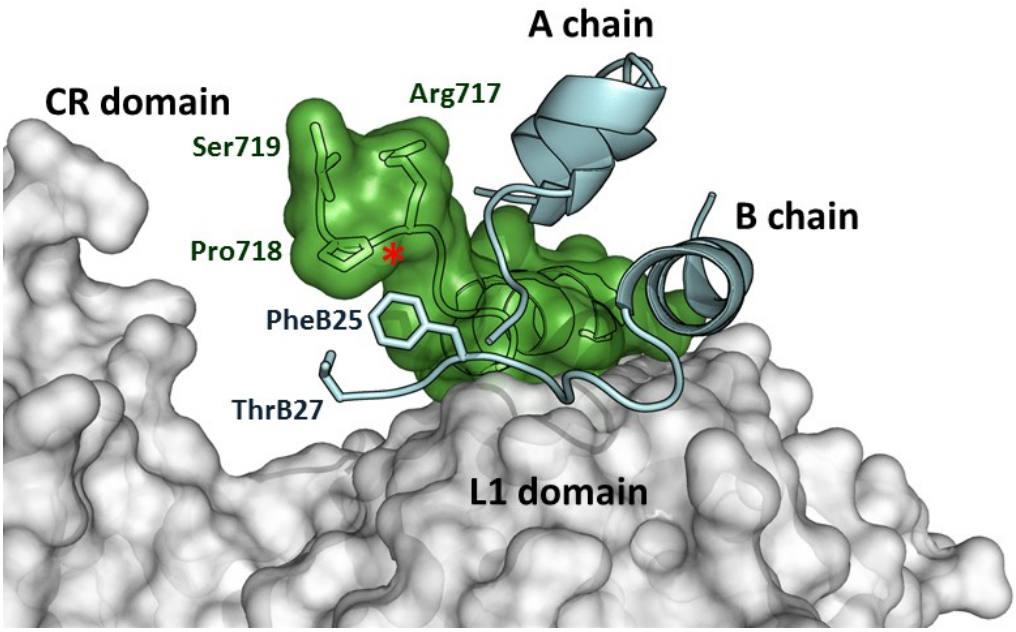

Figure 6. Detailed view of the C-terminus of the α-CT-A (in green) interacting with the receptor L1 domain (in grey) and insulin A- and B- chains (in cyan, B chain residues B28-B30 are not visible in the complex). The adjacent CR domain of the receptor is also shown (in grey). Side chains of some IR and insulin residues are shown as well. The red asterisk shows the insertion site for 12 extra amino acids of α-CT-B. The figure was created in PyMol from the PDB ID 4OGA structure. Reproduced from Ref. [46].

As already mentioned, IR has two equivalent binding sites for insulin per receptor homodimer and they are assigned to respective binding sites on insulin molecule described above. These binding sites in IR are referred as Site 1' and 1'' and Site 2' and 2'' [29]. Under normal physiological circumstances, IR is able to bind effectively only one molecule of insulin (Figure 7, page 17). Binding of one insulin molecule to IR destabilizes the second binding site on IR. However, at very high insulin concentrations, IR can bind theoretically up to 3 molecules of insulin [29].

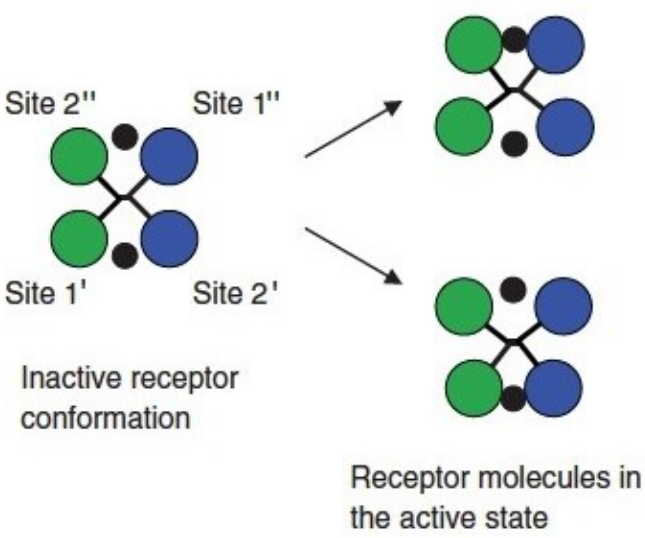

Figure 7. Mechanical display of insulin receptor binding mechanism. Green spheres represent one monomer, blue spheres show second monomer of the IR. Insulin is shown as a black ball. Individual binding sites on IR are labelled as 1', 2', 1'' and 2''. After crosslinking of one pair of Sites by insulin, receptor is activated. Reproduced from Ref. [29].

Binding of insulin leads to crosslinking of individual monomers, which induces a conformational change of the receptor (Figure 7 and 8) putting both intracellular tyrosine kinase subunits closer together and thus enabling their mutual autophosphorylation (i.e. activation). On the other hand, in the absence of insulin, IR should adopt an inactive, more open conformation. Interestingly, a recent article [30] published the first visualisation of full-length glycosylated human IR reconstituted in lipid nanodiscs by single-particle electron microscopy (Figure 8, page 18).

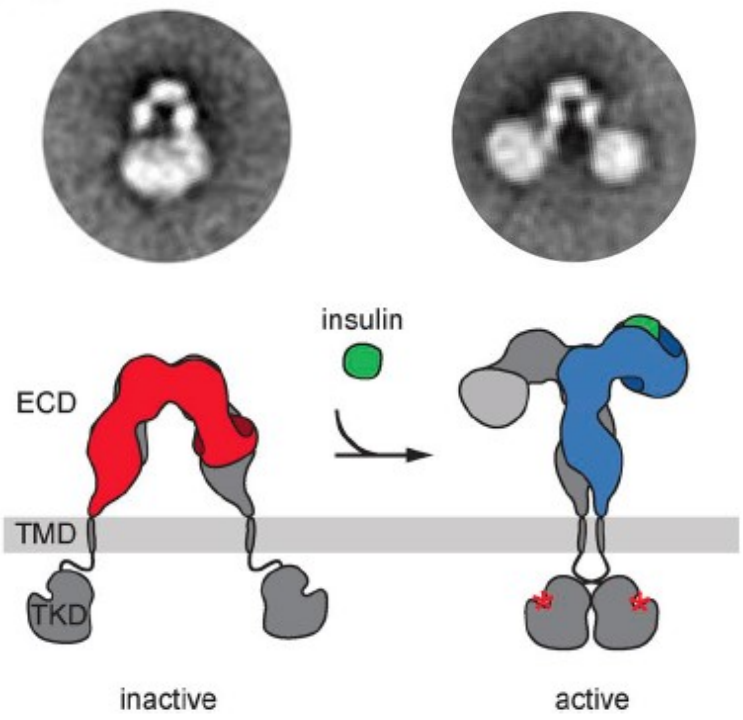

Figure 8. Ligand-induced conformational changes in the full-length human insulin receptor reconstituted in nanodiscs as observed by single-particle electron microscopy. Above. The conformational changes in IR visualized with the electron microscopy. Below. Cartoon illustration of respective conformational changes in IR, which occur after insulin (in green) binding. The transmembrane domains are brought together, facilitating the phosphorylation of TK domains. In the absence of insulin, the transmembrane domains are separated. Left, inactive state. Right, active state. Red asterisks represent activated (phosphorylated) TK domains. Reproduced from Ref. [30].

1.4. Autophosphorylation of the receptor and signalling pathway

After insulin binding, the IR, as it is a tyrosine kinase, activates and phosphorylates itself. This subsequently leads to a phosphorylation of receptor substrate (IRS) proteins (Figure 9), which are linked with activation of two main IR signalling pathways [31].

1.4.1. Metabolic actions of insulin

The first of the signalling pathways is a phosphatidylinositol-3-kinase (PI3K)-AKT/protein kinase B (PKB) pathway (see Figure 9, page 19), which is considered to be responsible for a majority of metabolic actions of insulin.

First, as already mentioned, IR and consequently IRS phosphorylation occur. Subsequently, activation of PI3K occurs, which then leads to the catalysis of the formation of phosphatidylinositol-3,4,5 triphosphate (PIP3) [32]. PIP3 then triggers the activation of 3-phosphoinositide-dependent kinase 1 (PDK1) and other factors and as a result, PDK1/2 activates AKT enzyme by phosphorylating its Thr308 and Ser473 residues [33]. The pathway is terminated by the dephosphorylation of IR by protein tyrosine phosphatase 1b (PTP1b) and tyrosine protein phosphatase non-receptor type 2 (PTPN2).

Downstream target of the AKT is the activation of AS160 responsible for glucose transporter 4 (GLUT 4) translocation to the cell membrane followed by a glucose uptake [34][35]. Aside from a regulation of glucose uptake, AKT is also responsible for increased glycogen synthesis through activation of glycogen synthase kinase-3 (GSK3) [36] and decreased gluconeogenesis by phosphorylation of forkhead box O1 (FOXO1) [37]. AKT is therefore a key enzyme in regulation of metabolic actions of insulin through the phosphorylation of several other substrates [38][35] (Figure 9).

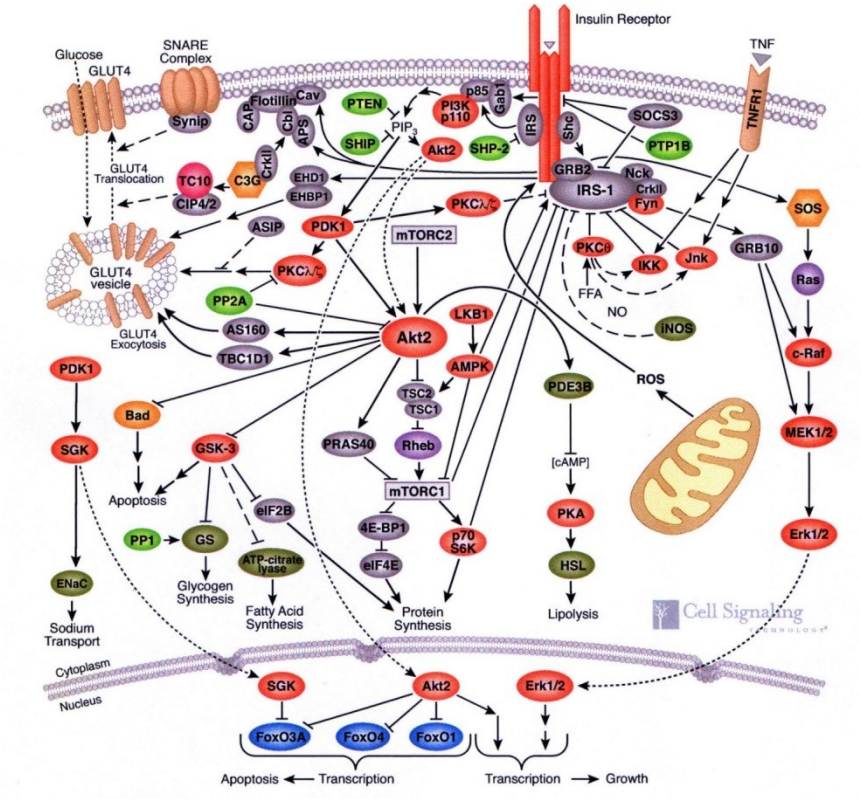

Figure 9. Signalling pathways of IR. Reproduced from Cell Signaling L.L.C.

1.4.2. Growth actions of insulin

The second IR signalling pathway is MAPK/ERK pathway (also known as the Ras-Raf-MEK-ERK pathway), which is responsible for growth and mitogen actions of insulin (see Figure 9). This pathway begins also with insulin binding to IR and its autophosporylation followed by IRS activation. IRS then functions as a docking protein to Src-homology-2-containing protein (Shc). Shc is phosphorylated and binds to Growth-factor-receptor-bound protein-2 (Grb 2) and Son-of-sevenless (SOS) resulting in Shc-Grb2-SOS complex [39]. SOS translocates from cytosol to plasma membrane and activates small GTPase Ras and subsequently Raf [32]. This cascade triggers activation of Mitogen-activated protein kinase (MEK1/2), which in turn phosphorylates Extracellular signal–regulated kinases (ERK1/2). The activated ERKs phosphorylate various targets and transcription factors, therefore promoting gene expression [40]. ERK is a key regulator in the mitogenic response to insulin and the IGFs, responsible for the cell growth, differentiation and cell survival [41].

1.5. Physiological action of insulin in comparison with insulin administration

Insulin is secreted from the pancreas, specifically from β-cells of Langerhans islets in response to increased blood glucose levels. Secretion of insulin is regulated by both hormonal and neural mechanisms, however, it is a very complex mechanism modulated by many other factors [42][43].

Under normal circumstances, a human body takes glucose from food. Postprandial glucose from intestine enters to the blood stream and it is subsequently recognized by β-cells of pancreas, which immediately release insulin into the portal vein. Endogenous insulin is first carried to the liver, where it inhibits gluconeogenesis and glycogenolysis. It is supposed that the liver clears up to 50% of secreted insulin. The rest of insulin is transported to the periphery of the body, where it enables entry of glucose (through activation of insulin dependent GLUT-4 transporter, see above) from the bloodstream to the adipose and muscle tissue [44]. Entry of glucose into the liver is mediated by GLUT-2 transporter, which is not insulin dependent [45].

Inhibition of gluconeogenesis and glycogenolysis by insulin in the liver is a crucial step in the glycaemic regulation and, when impaired, it is the main driver of elevated blood glucose in type 2 diabetes mellitus [44][46].

On the other hand, during subcutaneous administration to diabetic patients, insulin first acts on the periphery of the body and reaches the liver only later. This is in clear contrast to its normal physiological action and this can cause delayed inhibition of *de novo* gluconeogenesis in the liver and therefore, problems with glycaemic control, especially causing peripheral hyperinsulinemia, under-insulinization of the liver and glycaemic fluctuations [44][47].

Due to the fact that the liver contains > 90% of IR-B and most of the peripheral tissues much less, IR-B selective analogue could act preferably in the liver and better maintain normal physiological glycaemic levels [27][44]. Novo Nordisk team proved that this hypothesis may be realistic as they prepared and tested relatively moderately IR-B specific insulin analogues with IR-B/IR-A binding ratio about 3-5 but this specificity was sufficient to elicit primarily IR-B specific effects in vivo in rats [48].

2. The aims of the diploma thesis

- Prepare the following new insulin analogues (Figure 10):
  - Analogue **1**: Carboxyamidated insulin at the C-terminus of the B-chain (carboxyamide(B30)-insulin)
  - Analogue **2**: Carboxamidated insulin at the C-terminus of the B-chain with Gly at B31 (GlyB31-carboxyamide(B31)-insulin)
  - Analogue **3**: Carboxyamidated insulin at the C-terminus of the B-chain with Gly-Gly at B31-B32 (GlyB31-GlyB32-carboxymide(B32)-insulin)
  - Analogue **4**: Carboxyamidated insulin at the C-terminus of the B-chain with Gly-Gly-Gly at B31-B32-B33 (GlyB31-GlyB32-GlyB33-carboxymide(B33)-insulin)

- Determine binding affinities of new analogues for IR-A, IR-B and, if possible, for IGF-1R as well
- Test abilities of new analogues to induce autophosphorylation of IR-A and IR-B

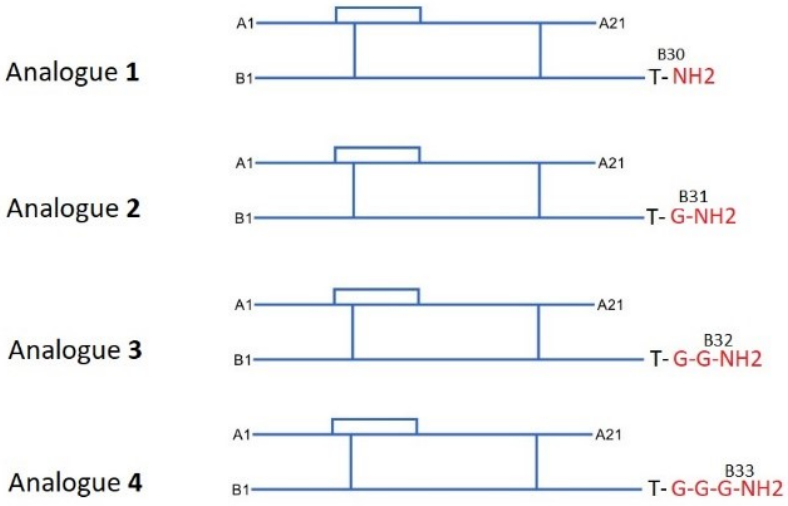

Figure 10. Schematic structures of new analogues planned in this work. Insulin chains A1-A21 and B1-B30 are shown as blue lines. Disulphide bridges are shown as blue lines as well. Planned changes are shown in red. Selected amino acids are shown in one letter codes (T or G) and NH_2 means C-terminal carboxyamide.

3. Material

3.1. Chemicals

4-Me-piperidine – Sigma-Aldrich, USA

HAc 99% – Penta, Czech Republic

Acetone – Penta, Czech Republic

ACN – Fischer Scientific, UK

Acrylamide – Fluka, Switzerland

Anti-Actin (20-33), IgG Fraction of Antiserum – Sigma-Aldrich, Germany

APS – Sigma-Aldrich, USA

BSA – Sigma-Aldrich, USA

Bromophenol blue – Sigma-Aldrich, USA

Cell line R^{+39} – a gift from prof. Antonino Belfiore (University of Catanzaro, Italy)

Cell line R^{-}/IR-A – a gift from prof. Antonino Belfiore (University of Catanzaro, Italy)

Cell line R^{-}/IR-B – a gift from prof. Antonino Belfiore (University of Catanzaro, Italy)

Cell line IM-9 – a gift from prof. Antonino Belfiore (University of Catanzaro, Italy)

1,4-butanediol – Fluka, Switzerland

Calcium acetate – Fluka, Switzerland

Diethyl ether – Penta, Czech Republic

DBU – Sigma-Aldrich, USA

DCM – Penta, Czech Republic

DIC – Sigma-Aldrich, USA

DIPEA – Sigma-Aldrich, USA

DMA – Fluka, Switzerland

DMF – Macron Fine Chemicals, USA

DMSO – Penta, Czech Republic

DODT – Tokyo Chemical Industry, Japan

DOI – prepared in group of Dr. Jiráček

DTT – Sigma-Aldrich, USA

Sodium lauryl sulfate – Sigma-Aldrich, USA

EDTA – Lachema, Czech Republic

Fmoc-protected amino acids – Novabiochem, Switzerland

Glucose – Sigma-Aldrich, USA

Glycerol – Sigma-Aldrich, USA

HEPES – Sigma-Aldrich, USA

HOBt – Sigma-Aldrich, USA

HI – Novo Nordisk (Denmark)

Human IGF-1 –Tercica, USA

Human IGF-2 – Sigma-Aldrich, USA

L-glutamine – Gibco, USA

Mono-^{125}I-TyrA14-human insulin – Perkin Elmer Life Sciences, USA

Mono-^{125}I-TyrA14-human IGF-1 – Perkin Elmer Life Sciences, USA

Medium DMEM – Gibco, USA

N-methylmorpholin – Sigma-Aldrich, USA

NMP – Merck, USA

Peroxidase antibody produced in mousse – Sigma-Aldrich, USA

Peroxidase antibody produced in rabbit – Sigma-Aldrich, USA

Phenol – Sigma-Aldrich, USA

Phospho-Akt (Thr308) (C31E5E) Rabbit mAb – Cell Signaling Technology, USA

Phospho-p44/42 MAPK (Erk1/2) (Thr202/Tyr204) (E10) Mouse mAb – Cell Signaling Technology, USA

Phospho-IGF-1 Receptor β (Tyr1135/1136) / Insulin Receptor β (Tyr1150/1151) (19H7) Rabbit mAb – Cell Signaling Technology, USA

Ponceau S – Sigma-Aldrich, USA

Potassium chloride – Lachema, Czech Republic

Puromycin – Gibco, USA

PVDF membrane – Millipore, USA

Calcium acetate - Fluka, Switzerland

FBS – Gibco, USA

Thioanisole – Fluka, Switzerland

TEMED – Sigma-Aldrich, USA

TFA – Fluka, Schwitzerland

Tris/HCl – Sigma-Aldrich, USA

TIS – Sigma-Aldrich, USA

TCEP – Sigma-Aldrich, USA

Trypsin – Sigma-Aldrich, USA

Tween 20 – Sigma-Aldrich, USA

Fmoc-Rink Amide AM resin – Novabiochem/Merck, Switzerland

Sodium chloride – Penta, Czech Republic

Sodium hydroxide – Penta, Czech Republic

SuperSignal™ West Femto Maximum Sensitivity Substrate – Thermo Fisher Scientific, USA

Other chemicals commonly used in the laboratory were supplied from Sigma-Aldrich, USA, Invitrogen, USA, Thermo Scientific, USA and Fluka, Switzerland.

3.2. Instruments

CCD camera ChemiDoc MP Imaging System – Bio-Rad, USA

Centrifuge CR3i – Jouan, USA

CO_2 Incubator MCO 180 AIC – Sanyo, Japan

Wizard 1470 Automatic Gamma Counter – Perkin Elmer, USA

6105 UV/VIS Spectrophotometer – Jenway, UK

Trans-Blot SD Semi-Dry Transfer Cell – Bio-Rad, USA

Biorad PowerPac 1000 Electrophoresis Power Supply – Bio-Rad, USA

RP-HPLC instrument Waters 600 – Waters Millipore (USA)

Elmasonic S 30 Ultrasonic Unit – Elma, Germany

Rotary Evaporator Heidolph WB 2000 – Heidolph, Germany

Automatic Synthesizer Spyder Mark II – functional prototype, IOCB

Heto PowerDry LL1500 Freeze Dryer – Thermo Fisher Scientific, USA

Thermo Fisher Scientific LTQ Orbitrap XL – Thermo Fisher Scientific, USA

3.3. Software

Image-Lab™ Software – Bio-Rad Laboratories, Inc., USA

Clarity Lite – Data Apex, Czech Republic

GraphPad Prism 5 – GraphPad Software, Inc., USA

4. Methods

4.1. Solid-phase synthesis of peptides

The four peptides (**1**-**4**) representing the C-terminus of the B-chain of insulin were prepared using the solid-phase peptide synthesis on Spyder Mark II Automatic Synthesizer.

- Peptide **1** – GFFYTPK(Pac)T-amide
- Peptide **2** - GFFYTPK(Pac)TG-amide
- Peptide **3** - GFFYTPK(Pac)TGG-amide
- Peptide **4** - GFFYTPK(Pac)TGGG-amide

The following protocol was used for all peptides prepared.

Preparation of the peptides was carried out by a standard solid-phase synthesis using Fmoc protected amino acids. The synthesis was performed from C-terminus end to N-terminus of the peptide. Fmoc-Rink Amide AM resin was used for the generation of the C-terminal amide. The amino acid side chains were protected with standard tBu, Boc and Trt protecting groups. Only Lysine N^{ε}-amino group was protected by Pac group and the amino acid was prepared in our laboratory [49]. The syntheses were carried out in a 200 μmol scale. The amino acids were dissolved in 7.6% (w/v) HOBt in DMF. The molarity of each amino acid used was 0.5 M. DIC in DMF (0.5 M) was used as an activation agent. Each condensation cycle was done twice and with 10 molar equiv. of Fmoc-amino acid and DIC in respect to the molar amount of the resin. The reaction time for one coupling was 45 minutes. For a deprotection of Fmoc group we used 2% DBU (v/v) and 20% (v/v) 4-Me-piperidine in DMF. Each deprotection cycle was done for 2 x 2 minutes. After coupling and deprotection cycles the resin was washed 5 times with 1.5 ml of DMF.

After the completion of the synthesis (about 24 hours) the resin with peptide was transferred from the synthesizer reactor to a flask and well washed with DCM. The resin was then dried in desiccator for 20 minutes. Subsequently, the resin was poured with 10 ml of the cleavage mixture containing TFA/deionized water/TIS in ratio 96/2/2 and the reaction mixture was stirred at room temperature for 2 hours. The cleavage mixture was filtered through a frit (S3) to the ice-cold diethyl ether (90 ml). Subsequently, the precipitate was centrifuged at 8000 x g for 11 minutes at 5 °C. The precipitated peptide was washed 4 times with 100 ml of ice-cold diethyl ether and was dried.

Each crude peptide was dissolved in 40% (v/v) acetonitrile in water with 0.1% (v/v) TFA and purified using RP-HPLC with preparative column C18 at the flow rate 9 ml/min (see 4.4).

Peptide identity was verified using mass spectrometry (discussed in 4.5) and purity by analytical RP-HPLC.

4.2. Enzymatic semisyntheses of insulin analogues' precursors

Analogues' precursors (precursors **1**-**4**) were prepared by the enzymatic semisyntheses using previously prepared peptides **1**-**4** and des(B23-B30)octapeptide insulin (DOI).

The following workflow was used for each precursor preparation.

Peptide was dissolved in 55% (v/v) DMF in 0.05 M calcium acetate and then DOI and trypsin were added. The first sample (1 μl) was taken to monitor initial conditions of the reaction by RP-HPLC and then the reaction pH was adjusted with few microliters of N-methylmorpholine to 6.9-7.0. The details are given in Table 1 (page 28).

The reaction mixture was stirred in RT and the samples were regularly taken (each of 1 μl) to monitor the course of the reaction using analytical RP-HPLC. After few hours (see Table 1), the reaction was stopped by adding acetone. The reaction mixture was then centrifuged for 10 minutes at 13,000 g, the precipitate was dissolved in 10% (v/v) HAc and purified with RP-HPLC (section 4.4).

The molecular weight and analogue precursor identity was confirmed using mass spectrometry (discussed in 4.5) and purity by analytical RP-HPLC.

Table 1. Experimental details for individual enzymatic semisynthesis of precursors of analogues.

Peptides used for individual semisynthesis	Amount of peptide (μmol)	Amount of DOI (μmol)	Amount of trypsin (μmol)	Total volume (μl)	Reaction time (hours)
Peptide **1** GFFYTPK(Pac)T-NH_2	30	6	0.12	210	4
Peptide **2** GFFYTPK(Pac)TG-NH_2	16	3.2	0.09	106	23
Peptide **3** GFFYTPK(Pac)TGG-NH_2	30	6	0.14	200	24
Peptide **4** GFFYTPK(Pac)TGGG-NH_2	29	5.9	0.21	195	23

4.3. Enzymatic deprotection of precursors of insulin analogues

After the enzymatic semisyntheses, it was necessary to remove phenylacetyl protecting groups from lysines of all analogues' precursors.

Individual analogues' precursors were dissolved (about 2.4 mg/ml) in 50 mM potassium phosphate buffer (pH 7.5). The reaction was started by the addition of penicillin amidohydrolase (aliquoted from Fluka, 10 IU in 6.6 μl of the buffer). The reaction mixture was stirred in RT and if needed (slow cleavage) in 37°C. During the reaction, samples (1μl) were taken to monitor the reaction using RP-HPLC.

After completed deprotection, the analogue was purified using RP-HPLC (section 4.4). The molecular weight and analogue identity was confirmed using mass spectrometry (discussed in 4.5) and purity by analytical RP-HPLC.

4.4. Reverse-phase liquid chromatography

For the purification of peptides after the solid-phase synthesis, the preparative column Nucleosil 120-5-C18 (250x21 mm) at flow rate 9 ml/min was used.

Insulin analogues and their precursors were purified using a semi-preparative column Nucleosil 120-5 C18 (250x10 mm) at flow rate 3 ml/min.

Nucleosil 120-5 C18 analytical column (250x4 mm) was used for the analysis of purified insulin analogues and precursors and for monitoring of reactions. The flow rate was 1 ml/min.

In each case, 0.1% (v/v) TFA in deionized water was used as a mobile phase A and 0.1% (v/v) TFA with 80% (v/v) ACN in deionized water as a mobile phase B. Mobile phases A and B were mixed according to gradients described in Tables 2 and 3.

Table 2. Gradient 1 used for the purification of peptide precursors. Absorbance was detected at 218 nm and 276 nm. The flow rate was 9 ml/min.

Gradient 1			
Time [min]	0	30	31
Concentration of mobile phase B solution in % (v/v)	10%	100%	10%

Table 3. Gradient 2 used for purification of analogues and analogue precursors. Absorbance was detected at 218 nm at 276 nm. Flow rate was 3 ml/min. The same gradient was also used for analytical RP-HPLC at flow rate 1 ml/min.

Gradient 2							
Time [min]	0	1	21	34	36	37	37,1
Concentration of mobile phase B solution in % (v/v)	10%	35%	45%	55%	90%	90%	10%

4.5. Mass spectrometry

For the identification of peptides, insulin analogues and their precursors, the mass spectrometry analyses were performed in the Mass Spectrometry Laboratory of IOCB AS CR. Mass spectrometry was carried out using the Thermo Fisher Scientific LTQ Orbitrap XL with method ESI (electrospray ionization) in positive ion mode.

4.6. Binding studies of the ligands *in vitro*

Testing of the binding affinities of the insulin analogues to individual receptors was performed as a competition for binding sites on the individual receptors between the tested ligand and ^{125}I-labelled insulin when tested for the affinity to IR or the ^{125}I- labelled IGF-1

when tested for the affinity to IGF-1R. The assays were carried out at a constant number of cells, a constant concentration of radiolabelled insulin and with different concentrations of studied ligands.

4.6.1. Preparation of ligand solutions for the binding assays

First, the stock solutions (100 μg/ml in 0.1% HAc) of individual ligands were prepared. The exact concentrations were determined using spectrophotometric measurement of the absorbance at 280 nm. The extinction coefficient for all ligands including the human insulin was 5840 $M^{-1}.cm^{-1}$ and was calculated from equation ε = (nY x 1280) + (nC x120), where nY stands for number of the tyrosine residues and nC stands for number of the cysteines. Before the binding assays, the stock solutions of ligands were diluted to 10^{-5} - 10^{-11} M with 100 mM HEPES, 100 mM NaCl, 5 mM KCl, 1.3 mM $MgSO_4$, 1 mM EDTA, 10 mM glucose, 15mM sodium acetate and 1% (w/v) BSA.

4.6.2. Cultivation of cells for the determination of ligand binding affinity to IR-A

For a determination of the binding affinities of the ligands to IR-A, we used a cell line of human lymphocytes IM-9 expressing exclusively IR-A.

The cells were cultivated at 37 °C, in the presence of 5% CO_2, in RPMI 1640 medium containing 10% FBS, 100 units/ml penicillin, 100 μg/ml streptomycin and 2 mM L-glutamine. The cells were passaged three times a week. Cultivated cells were counted and then diluted with the binding buffer to concentration 2 million cells/ml.

4.6.3. Determination of the binding affinity of the ligands to IR-A

The cells were incubated with ^{125}I-insulin of the constant concentration (0.01 nM) and elevating concentration series of each ligand in the binding buffer (described in 4.6.1.). The incubation proceeded at 15 °C for 2.5 hours and the reaction tubes were stirred every 30 minutes. The total volume of the mixture was 500 μl. After the incubation, the duplicates (2 x 200 μl) were prepared from each reaction test-tube. Then, 200 μl of the cold binding buffer was added to each duplicate to terminate the reaction. The samples were centrifuged at 1,300 x g for 10 minutes at 4 °C. The supernatant was removed, and respective radioactive pellets were measured using a Wizard 1470 Automatic γ Counter. The measuring time per sample was 10 minutes.

Binding data were analysed using Excel software specially developed for IM-9 cells in the laboratory of P. De Meyts (Novo Nordisk A/S, Denmark). The software uses a method of non-linear regression with one-site fitting model and takes into account the possible free ligand depletion.

Each binding curve for an individual analogue was determined from duplicate points and for each analogue at least 3 binding curves were determined (n = 3). The final dissociation constant of an analogue was calculated from all binding curves measured. The K_d of ^{125}I-insulin (0.3 nM) was determined previously in the laboratory of J. Jiráček.

4.6.4. Preparation of cells to determine the binding affinity of the ligands to IR-B and IGF-1R

For the determination of binding affinities to IR-B, the cell line R^-/IR-B (mouse embryonic fibroblasts with knocked out mouse IGF-1R gene and transfected with human IR-B gene) was used.

For the determination of binding affinities to IGF-1R, the R^{+39} cell line (mouse embryonic fibroblasts with knocked out mouse IGF-1R gene and transfected with human IGF-1R gene) was used.

The cells were cultivated at 37 °C, in the presence of 5% CO_2, in medium DMEM containing 10% FBS, 100 units/ml penicillin, 100 μg/ml streptomycin, 3 μg/ml puromycin, 25 mM glucose and 2 mM L-glutamine. The cells were passaged three times a week. Cultivated cells were seeded into the 24-well plates in amount of 12,000 cells per well. They were grown in DMEM medium for 24 hours. After this period, the cells were starved for 4 hours in FBS-free medium and subsequently stimulated.

4.6.5. Determination of the binding affinity of ligands to IGF-1R and IR-B

The cells were left for 6 hours before testing in FBS-free medium to remove serum insulin. Medium was removed just before assay and each well was washed with 2 x 300 μl of the binding buffer (described in 4.6.1.).

The cells were incubated with ^{125}I- ligand of the constant concentration (0.043 nM ^{125}I-insulin in case of IR-B or 0.039 nM ^{125}I-IGF-1 in case of IGF-1R) and a concentration series of each ligand in the binding buffer (described in 4.6.1.). The incubation proceeded at 5 °C for 16 hours and the reaction plates were continuously stirred during the reaction. The total volume per well was 250 μl, and each sample was prepared in duplicates. After the

incubation, the samples with cells were washed with 2 x 300 μl of the cold binding buffer and then the cells were treated with 2 x 300 μl 0.1 M NaOH. The solubilised cells were transferred into the tubes and the radioactive signal was measured using a Wizard 1470 Automatic γ Counter. The measuring time per sample was 1 minute.

The binding curves were analysed using GraphPad Prism 5 software using a method of non-linear regression for one-site fitting model and taking into account the possible free ligand depletion. Each binding curve for an individual analogue was determined from duplicate points and at least 3 binding curves were determined (n = 3) for each analogue. The final dissociation constant of an analogue was calculated from all binding curves measured. The K_d of ^{125}I-insulin (0.3 nM) and of ^{125}I-IGF-1 (0.2 nM) was determined previously in the laboratory of J. Jiráček.

4.7. Study of abilities of ligands to induce autophosphorylation of the receptors and subsequent signalling

4.7.1. Preparation of the cells for the study of the activation of IR-A, IR-B and IGF-1R

For the study of the activation of IR-A, IR-B and IGF-1R, the cell lines R^-/IR-A, R^-/IR-B and R^{+39} respectively, were used. Individual cell lines are mouse embryonal fibroblasts with knocked out gene for mouse IGF-1R and transfected with human IR-A, IR-B and IGF-1R gene.

The cells were cultivated at 37 °C, in the presence of 5% CO_2, in DMEM medium (described in 4.6.4.) and then seeded into the 24-well plates in amount of 40,000 cells per well for cell line R^{+39} and the same number of per well for cell lines R^-/IR-A and R^-/IR-B. They were grown in DMEM medium for 24 hours. After this period, the cells were starved for 4 hours in FBS-free medium and subsequently stimulated.

4.7.2. Preparation of ligand solutions for the cell receptors stimulation

The ligands were diluted in FBS-free medium into two distinct concentrations; 10 nM and 1 nM. The exact concentrations were determined spectrophotometrically at 280 nm. The extinction coefficient of all ligands was 5840 $M^{-1}.cm^{-1}$ and was calculated as described previously in 4.6.1.

4.7.3. Stimulation of IR-A, IR-B and IGF-1R by individual ligands

The ligands were added to the medium and respective cells (cell lines R^-/IR-A, R^-/IR-B and R^{+39} for stimulation of IR-A, IR-B and IGF-1R respectively) in each well for 10 minutes. Solution of ligands were tested in two concentrations, 10 nM and 1 nM. After the stimulation the reaction was terminated by a removal of medium. The wells were washed with physiological solution (0.9% NaCl), poured with liquid nitrogen and frozen until the next manipulation. A control well without added ligand was prepared for each sample. Ligands were tested 4 times at each concentration using different batches of cells.

4.7.4. Preparation of cell lysates for SDS-electrophoresis

Cells in each well were lysed using lysis buffer consisting of 62.5 mM Tris/HCl (pH 6.8), 2% SDS (w/v), 10% glycerol (v/v), 0.01% Bromophenol Blue (w/v), 0.1 M DTT (w/v), 50 mM NaF, 1 mM Na_3VO_4 and 0.5% protease inhibitors. 50 µl of the lysis buffer was added to each well. Subsequently, cells were sonicated for 1 min. Cell lysates were then transferred into Eppendorf tubes and stored in -20°C.

4.7.5. SDS-PAGE electrophoresis of the cell lysate proteins

SDS-page electrophoresis of the cell lysate of proteins was performed using 10% SDS polyacrylamide gel. Before electrophoresis, all samples were heated at 100 °C for 1 min and 10 µl (12±2 µg, 11±1.5 µg and 8.3±0.8 µg of protein amount for cell lines R^-/IR-A, R^-/IR-B and R^{+39} respectively) of respective cell lysate was added to each well.

The electrophoretic separation was done in the presence of 0.025 M Tris/0.192 M glycine electrode buffer with 0.1% (w/v) SDS. Electric current was limited to 24 mA per gel. The electrophoresis was performed for 10 minutes at 100 V, then the voltage was increased to 200 V. The total electrophoretic separation time was about 1 hour.

4.7.6. Immunoblotting

After completion of the SDS-PAGE electrophoresis, we followed with the electro blotting of the cell lysate proteins from the gel to PVDF membrane. The gels were transported into the transfer buffer containing 20 mM Tris, 189 mM glycine, 10% methanol (v/v) and 0.1% SDS (w/v) and left there for 30 minutes. Before blotting, the PVDF

membranes were activated in methanol, washed with deionized water and then left for 20 minutes in the transfer buffer. Filter paper was soaked in the buffer as well. The electro blotting was done in semi-dry transfer cell and proceeded for 75 minutes. The constant voltage 12 V was set, and the limiting electric current was 1,5 mA per cm^2.

Next, PVDF membranes were reversibly stained with 0.1% Ponceau S to visualize proteins and membranes were cut in positions of molecular weight of standards to obtain parts with the target proteins (receptors between top to 75kDa, Akt between 75-50kDa and Erk bellow 50kDa). The membranes were left for 1 hour under constant stirring in 5% BSA in T-TBS (20 mM Tris/Cl- pH 7.5, 140 mM NaCl, 0.1% Tween-20 (v/v)) at RT. Membranes were then briefly washed with T-TBS and then incubated overnight in primary antibodies at 4 °C. The primary antibodies were diluted in 5% BSA in T-TBS.

The next day the membranes were washed with T-TBS for 3 x 5 min and then incubated for 1 hour with respective secondary antibodies conjugated with horseradish peroxidase. The secondary antibodies were diluted in 5% non-fat milk in T-TBS. After the incubation, the membranes were again washed with T-TBS for 3 x 5 min and then once more for 10 minutes. The antibodies used for detection of the proteins are given in Table 4 (page 35).

Then, we followed with the detection of the proteins on individual membranes. For the detection of the signal, the chemiluminiscent SuperSignal West FEMTO Max sensitivity substrate was used. The membranes were incubated with the substrate for 3 minutes and the chemiluminiscence was subsequently detected using CCD Camera ChemiDoc MP Imaging System. The signal intensity was quantified by Image-Lab software.

The intensity of the signal of each ligand was related to intensity of the signal of insulin (cell lines R^-/IR-A, R^-/IR-B) or IGF-1 (cell line R^{+39}) in a particular experiment. The data were later analysed using GraphPad Prism 5 software. The level of phosphorylation was calculated together with standard error of the mean (SEM) from 4 independent experiments.

Table 4. The antibodies used for detection of the proteins.

Detected protein	The name of the antibody	Dilution	Organism of origin
Primary antibodies			
pAkt	Phospho-Akt (Thr 308) (C31E5E) Rabbit mAb, Cell Signaling Technology, USA	1:1000	Rabbit
pErk	Phospho-p44/42 MAPK (Erk1/2) (Thr202/Tyr204) (E10) Mouse mAb, Cell Signaling Technology, USA	1:2000	Mouse
pTyr 1150/1151 IR	Phospho-IGF-1 Receptor β (Tyr1135/1136) / Insulin Receptor β (Tyr1150/1151) (19H7) Rabbit mAb Cell Signaling Technology, USA	1:1000	Rabbit
pTyr 1135/1136 IGF-1R	Phospho-IGF-1 Receptor β (Tyr1135/1136) / Insulin Receptor β (Tyr1150/1151) (19H7) Rabbit mAb Cell Signaling Technology, USA	1:1000	Rabbit
Control primary antibodies detecting total mass of protein			
Actin	Anti-Actin (20-33), IgG Fraction of Antiserum, Sigma-Aldrich, Germany	1:2000	Rabbit
Secondary antibodies			
Antibody recognizing primary antibody of rabbit origin	Anti-Rabbit IgG (whole molecule) Peroxidase antibody produced in goat, Sigma-Aldrich, Germany	1:80000	Goat
Antibody recognizing primary antibody of mouse origin	Anti-Mouse IgG (whole molecule) Peroxidase antibody produced in rabbit, Sigma-Aldrich, Germany	1:20000	Rabbit

5. Results

5.1. The solid-phase synthesis of the peptides

By solid-phase synthesis, four peptides (**1**-**4**) were synthesised in order to use them for the preparation of insulin analogues **1**-**4**, respectively.

By automated solid-phase synthesis, 107 mg of the crude peptide **1** was obtained. The amount of the crude peptide **2** was 231 mg, amount of the crude peptide **3** was 193 mg and amount of the crude peptide **4** was 251 mg.

All peptides were purified using RP-HPLC and peptide identification was performed by mass spectrometry. The representative chromatogram of peptide **1** purification is in Figure 11 and its MS spectrum is in Figure 12.

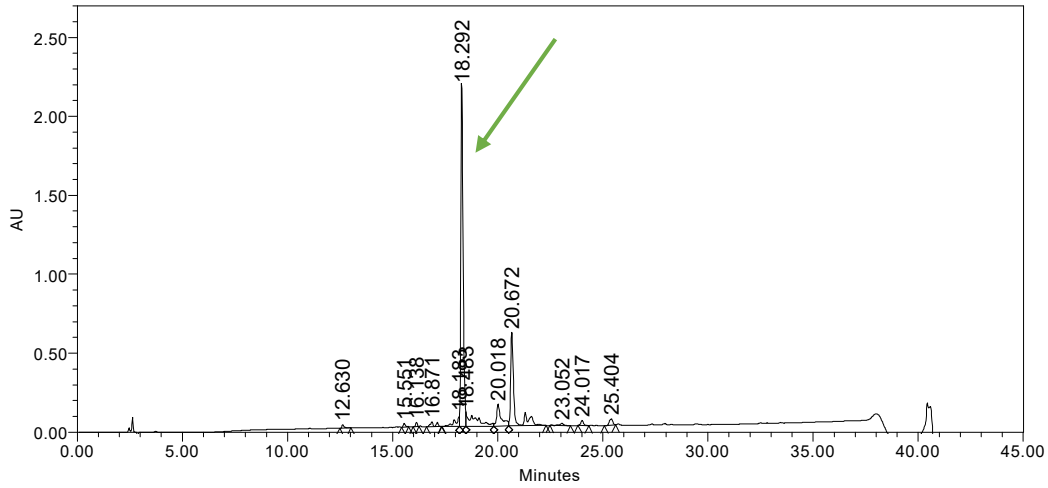

Figure 11. Chromatogram of the crude peptide **1**. Time 18.29 minute. The absorbance was detected at 218 nm. The peak of the peptide is marked by a green arrow.

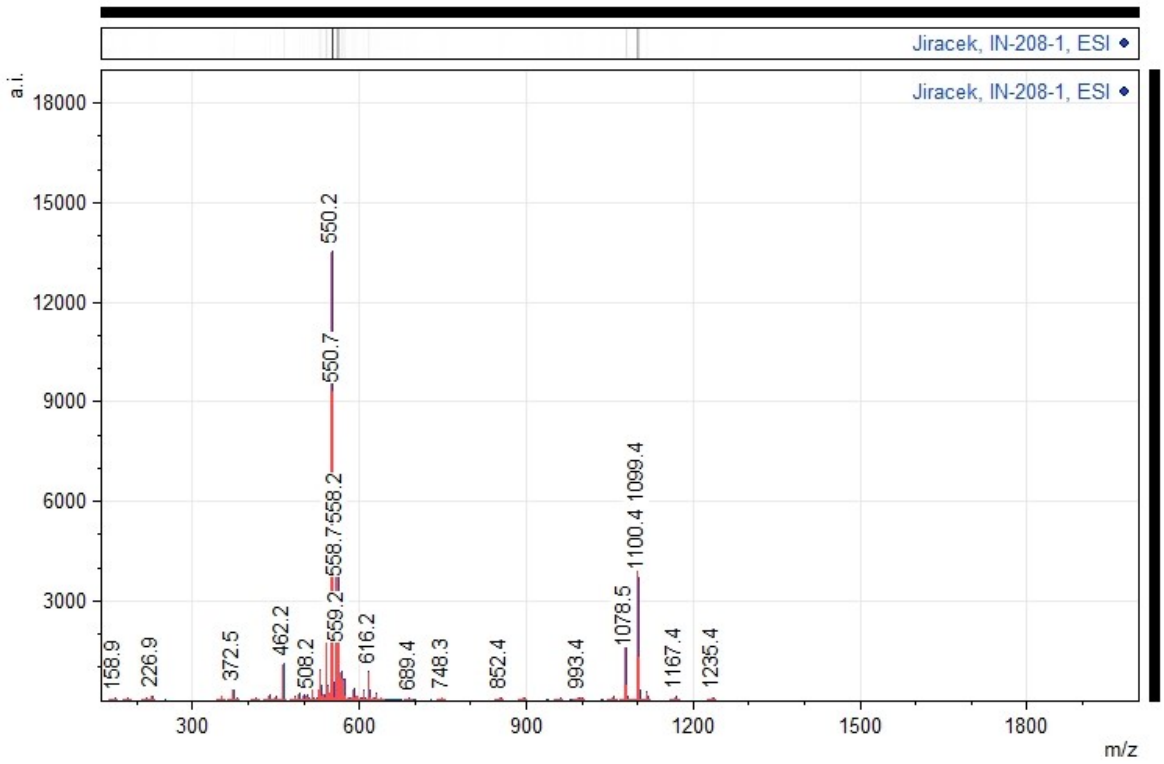

Figure 12. Mass spectrum of purified peptide **1** measured with ESI method (electrospray ionization). The theoretical relative molecular monoisotopic mass (Mr) is 1076.5331, which corresponds to m/z signal 1099.4 (product with Na adduct ion [M+Na^+]).

The final purified peptide **1** yielded 70.7 mg (65.7 μmol), corresponding to 32.8% yield, because the synthesis was performed in a 200 μmol scale. The amount of the final peptide **2** was 31.8 mg (28.1 μmol), corresponding to 48.2% yield. Peptide **3** was obtained in amount of 47.5 mg (39.9 μmol), equivalent to 56.3% yield and amount of peptide **4** was 36.9 mg (29.6 μmol), and the corresponding yield was 84.6%. The yields and MS data for HPLC-purified peptides **1**-**4** are shown in Table 5 (page 38).

Table 5. Experimental and theoretical relative monoisotopic molecular masses of prepared purified peptides and their yields after HPLC purification.

Peptide Amino acid sequence	Yield of the purified peptide (mg)	Amount of crude peptide for purification (mg)	Yield of the purified peptide (%)	Mr theoretical	Mr experimental
1 GFFYTPK(Pac)T-NH_2	71	107.3	32.8%	1076.5331	1076.4102
2 GFFYTPK(Pac)TG-NH_2	32	66	48.2%	1133.5546	1133.5100
3 GFFYTPK(Pac)TGG-NH_2	48	68.6	56.3%	1190.5760	1190.5776
4 GFFYTPK(Pac)TGGG-NH_2	37	43.6	84.6%	1247.5986	1247.5975

5.2. Enzymatic semisyntheses of the analogues

Peptides **1-4** were used for the enzymatic semisyntheses of analogues' precursors **1-4** described in Chapter 4.2. The course of the semisynthesis was continuously monitored by RP-HPLC. Identification of the analogue precursors was performed by mass spectrometry. In general, we observed that the progress of semisynthetic reactions was slower with the longer peptide chain. However, a sufficient amount of the product was obtained for all analogues.

After the completion of the semisynthesis, the mixture was analysed and purified with RP-HPLC. The representative chromatogram of the final reaction mixture for analogue precursor **1** is shown in Figure 13 (page 39).

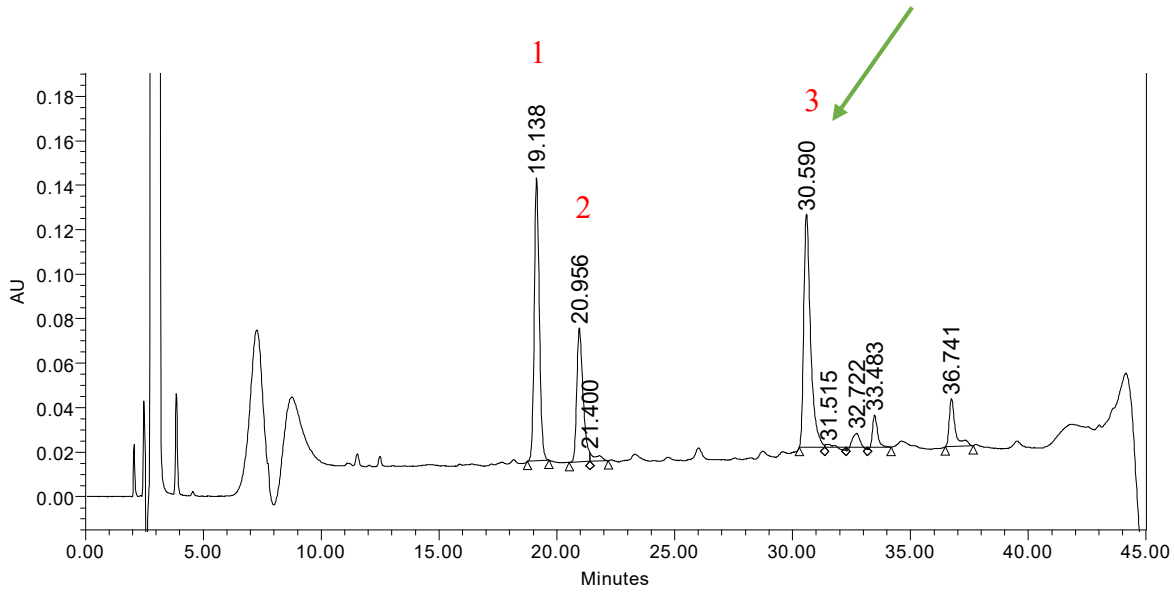

Figure 13. Chromatogram of the semisynthesis of the analogue precursor **1** after 3 h of the reaction. For clarity, the numbers of individual fractions are listed. Fraction 1 represents peptide **1**, fraction 2 is DOI. The product was in the fraction 3 indicated with the green arrow. Absorbance was monitored at 218 nm.

The product was further purified. The yields of HPLC purified analogue precursors altogether with their theoretical and experimental relative molecular masses are shown in the Table 6 (page 40).

Table 6. Relative monoisotopic molar masses of prepared analogue precursors and their yields. DOI is des(B23-B30)octapeptide insulin and the peptides represent the B-chain C-terminal sequences in insulin.

Analogue precursor	Amount of analogue precursor (mg)	Yield of analogue precursor (%)	Mr theoretical	Mr experimental
1 DOI-GFFYTPK(Pac)T-NH_2	8.3	23.8%	5920.6981	5920.7032
2 DOI-GFFYTPK(Pac)TG-NH_2	3.6	19.2%	5977.7169	5977.7252
3 DOI-GFFYTPK(Pac)TGG-NH_2	4	11.2%	6034.7387	6034.7501
4 DOI-GFFYTPK(Pac)TGGG-NH_2	1.1	3.1%	6091.7598	6091.7823

5.3. Enzymatic deprotection of the analogues' precursors

All purified precursors of analogues were subsequently deprotected (Pac group cleaved from the N^{ε} amino group of lysine) by penicillin amidohydrolase. The representative chromatogram of the reaction mixture during the enzymatic deprotection of analogue precursor **1** is shown in Figures 14 and 15 (page 41).

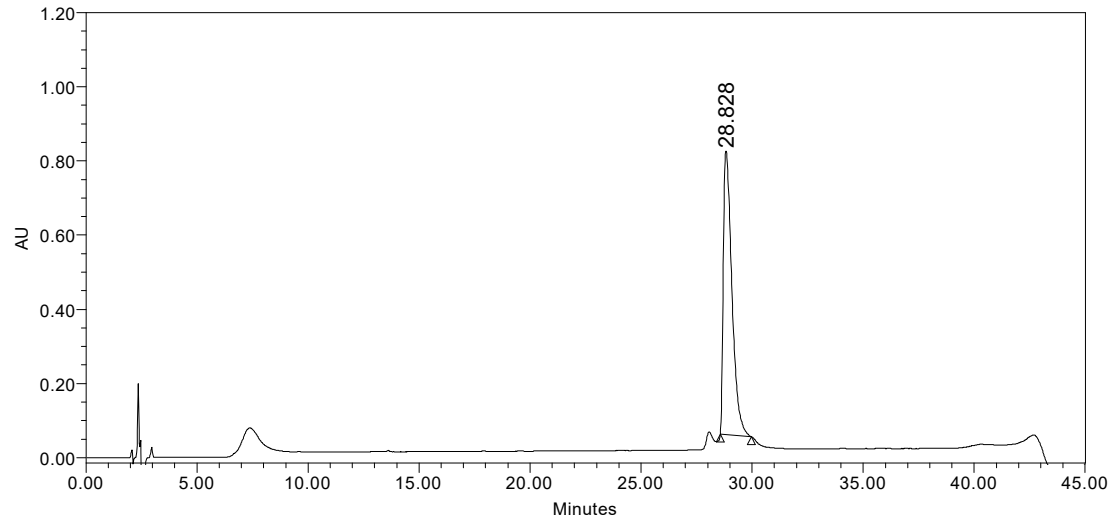

Figure 14. Chromatogram of the analogue **1** precursor before starting the deprotection reaction. The peak at time 28.828 minutes represents analogue **1** precursor with Pac protecting group present at the beginning of the reaction. Absorbance was monitored at 218 nm.

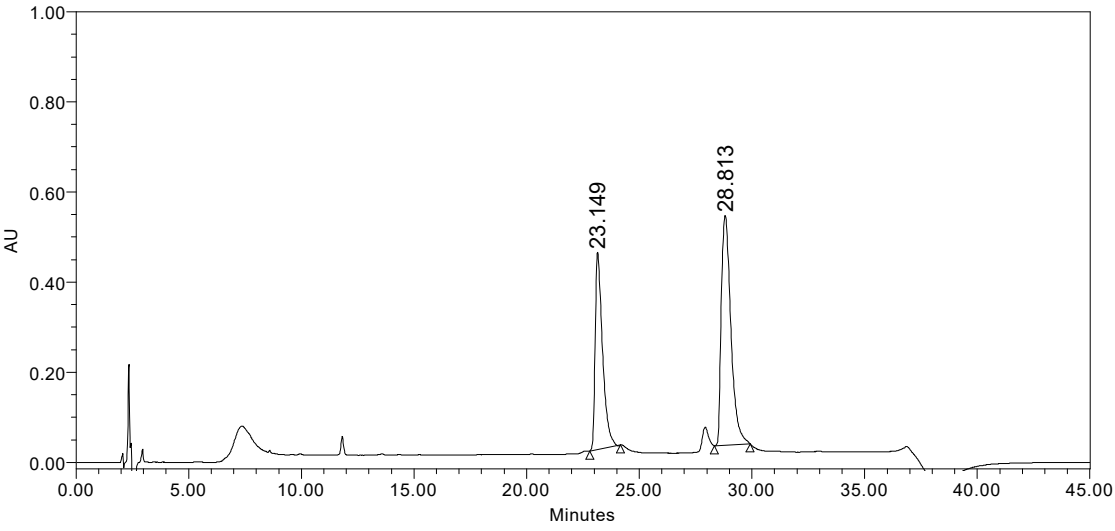

Figure 15. Chromatogram of the deprotection of analogue **1** precursor after 3h of the reaction. The peak at time 23.149 minutes represent deprotected insulin analogue **1**, peak at 28.813 represents analogue precursor **1**. Reaction time was 24 hours. Absorbance was monitored at 218 nm.

All final analogues **1**-**4** were purified and analysed by HPLC (Figures 16-19) and their identities verified by MS. The yields of HPLC purified analogues altogether with their theoretical and experimental relative molecular masses are shown in the Table 7, page 46.

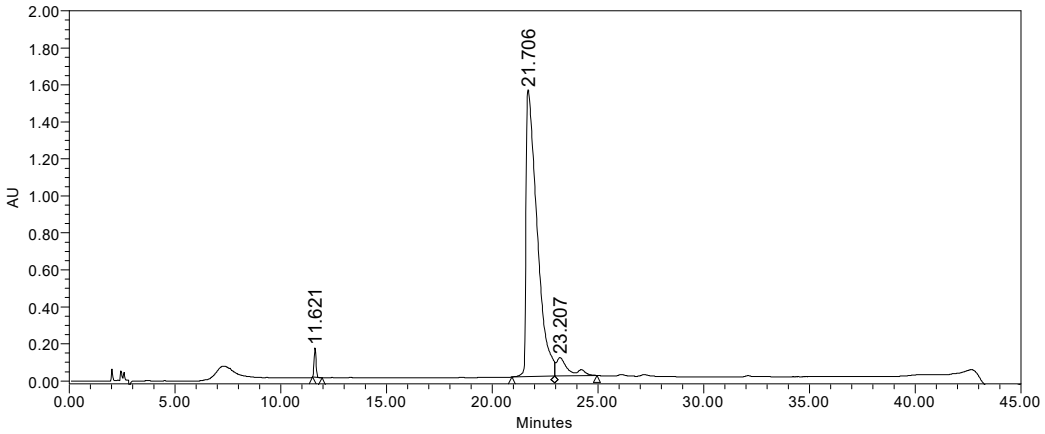

Figure 16. RP-HPLC analysis of the purified analogue **1**. Absorbance was monitored at 218 nm.

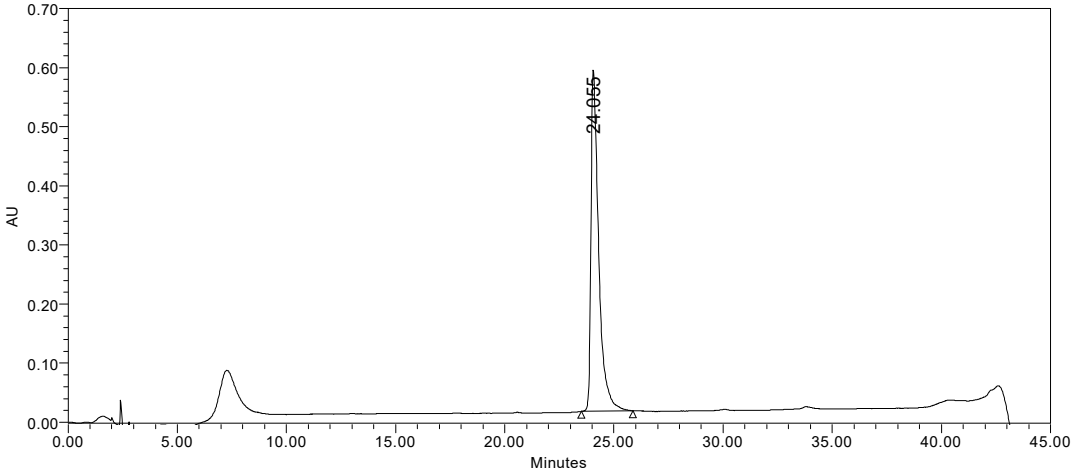

Figure 17. RP-HPLC analysis of the purified analogue **2**. Absorbance was monitored at 218 nm.

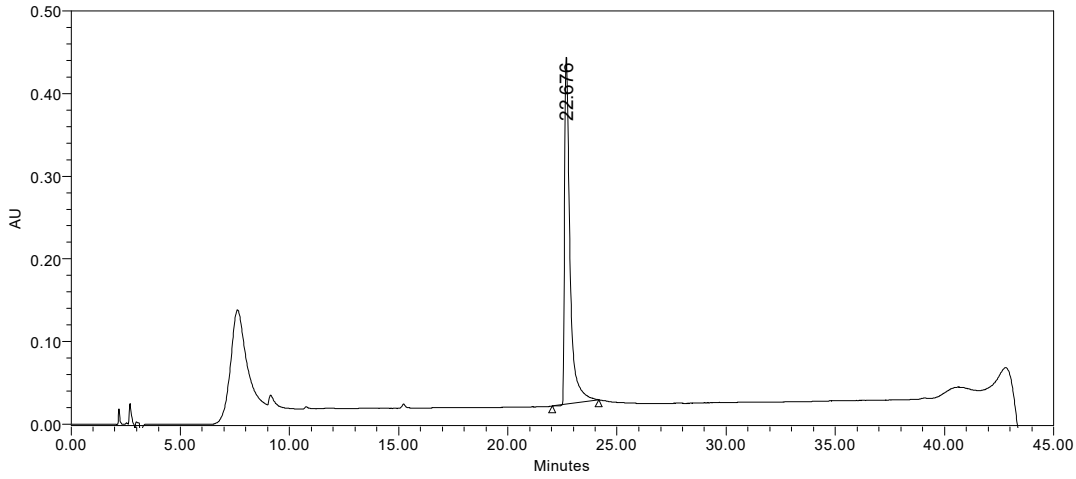

Figure 18. RP-HPLC analysis of the purified analogue **3**. Absorbance was monitored at 218 nm.

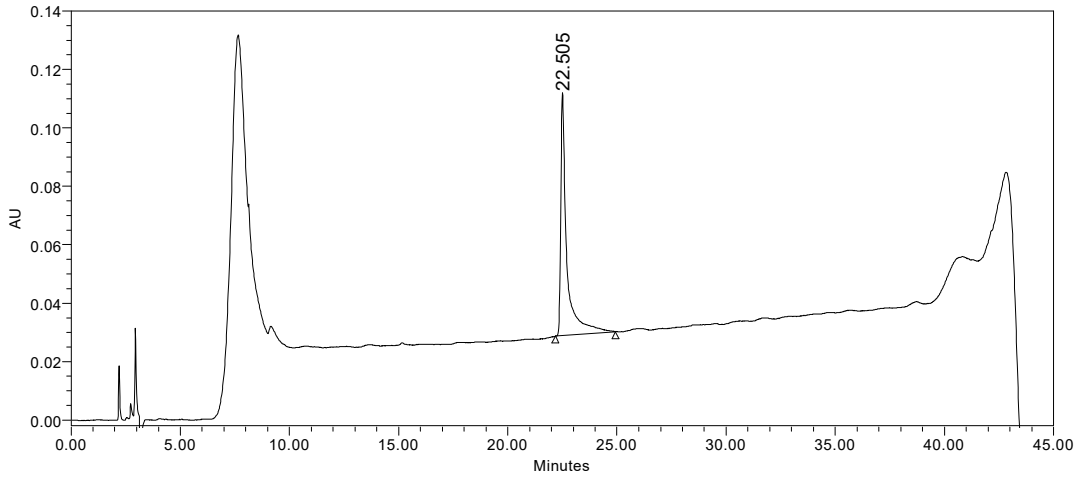

Figure 19. RP-HPLC analysis of the purified analogue **4**. Absorbance was monitored at 218 nm.

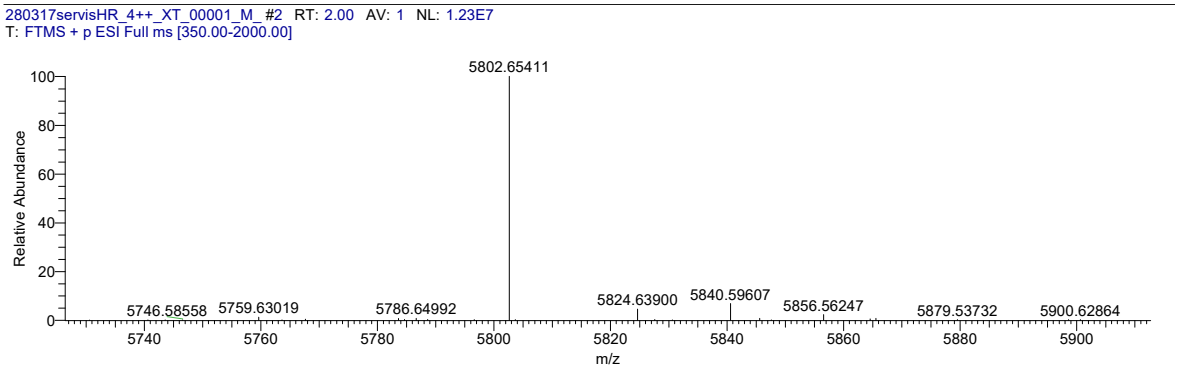

Figure 20. MS spectrum of the final analogue **1**. The theoretical relative molecular monoisotopic mass (Mr) is 5802.6562, which corresponds to the deconvoluted m/z signal 5802.6541.

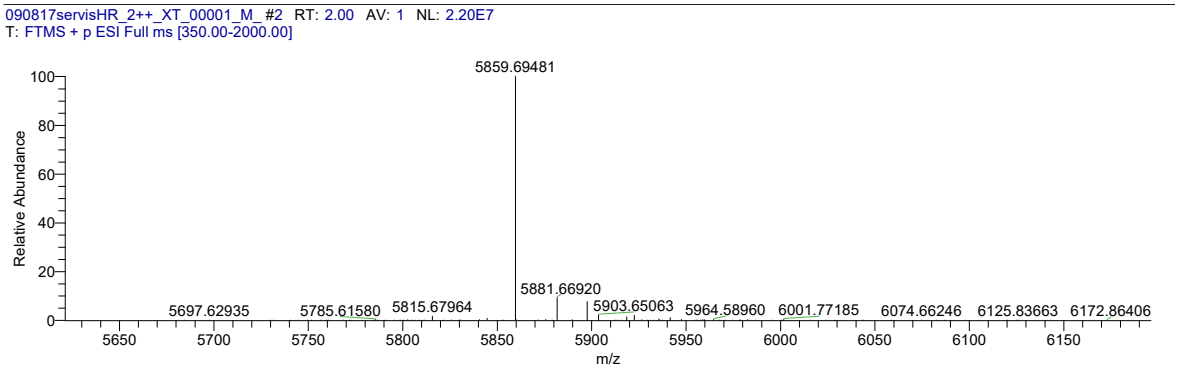

Figure 21. Mass spectrum of the final analogue **2**. The theoretical relative molecular monoisotopic mass (Mr) is 5859.675, which corresponds to the deconvoluted m/z signal 5859.6948.

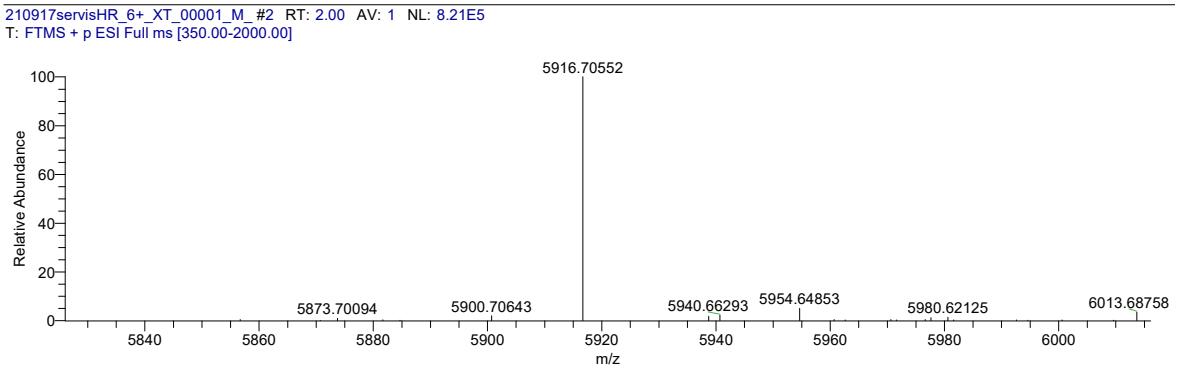

Figure 22. Mass spectrum of the final analogue **3**. The theoretical relative molecular monoisotopic mass (Mr) is 5916.6965, which corresponds to the deconvoluted m/z signal 5916.7055.

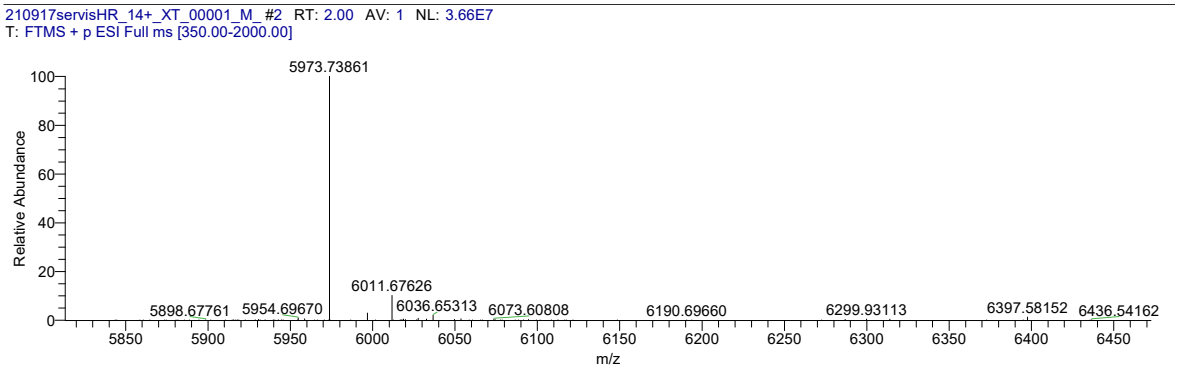

Figure 23. MS spectrum of the final analogue **4**. The theoretical relative molecular monoisotopic mass (Mr) is 5973.7183. The product corresponds to the deconvoluted m/z signal 5973.7386.

Overall, we can summarize that 5.5 mg of the analogue **1** (0.94 μmol) was obtained, corresponding to 15.8% yield. Next, 1 mg (0.17 μmol) of the analogue **2** was obtained, which corresponds to 5.3% yield. Analogue **3** was prepared in amount of 1.7 mg (0.29 μmol) and with 4.8% yield, and finally we obtained 0.3 mg (0.05 μmol) of the final analogue **4**, which corresponds to 0.9% yield. The relative molecular weights and yields are summarized in Table 7 (page 46).

Table 7. Relative molar masses of prepared analogues and their yields of their semisynthesis (semi) and deprotections (dePac).

Analogue	Yield of the final analogue (mg)	Yield of the final analogue (%)	Mr theoretical	Mr experimental
1 carboxamide(B30)-insulin	5.5	15.8% (semi) 66.3% (dePac)	5802.6562	5802.6541
2 GlyB31-carboxamide(B31)-insulin	1	5.3% (semi) 27.8% (dePac)	5859.675	5859.6948
3 GlyB31-GlyB32-carboxamide(B32)-insulin	1.7	4.8% (semi) 42.5% (dePac)	5916.6965	5916.7055
4 GlyB31-GlyB32-GlyB33-carboxamide(B33)-insulin	0.3	0.9% (semi) 27.3% (dePac)	5973.7183	5973.7386

5.4. Binding studies

After the purification of sufficient amounts of analogues **1**-**4**, we determined their binding affinities for IR-A and IR-B and the data were compared with binding affinities of human insulin. When testing the binding affinity to IR-A, insulin analogues were tested on the human lymphocyte cell line IM-9 expressing only IR-A, according to the procedure described in chapter 4.6.3. From the obtained data, binding curves were plotted using GraphPad Prism 5.

The binding assays of insulin analogues with IR-B were performed using the cell line of mouse embryonic fibroblasts with blocked expression of the IGF-1R mouse genes and transfected with human IR-B (R-/IR-B) as described in Chapter 4.6.5.

Finally, dissociation constants (K_d) of all insulin analogues were calculated from individual binding curves. Representative binding curves are shown in Figures 24-27. K_d values are shown in Table 8 (page 49). Relative binding affinities of analogues were calculated as relative to the binding affinity of human insulin (100%).

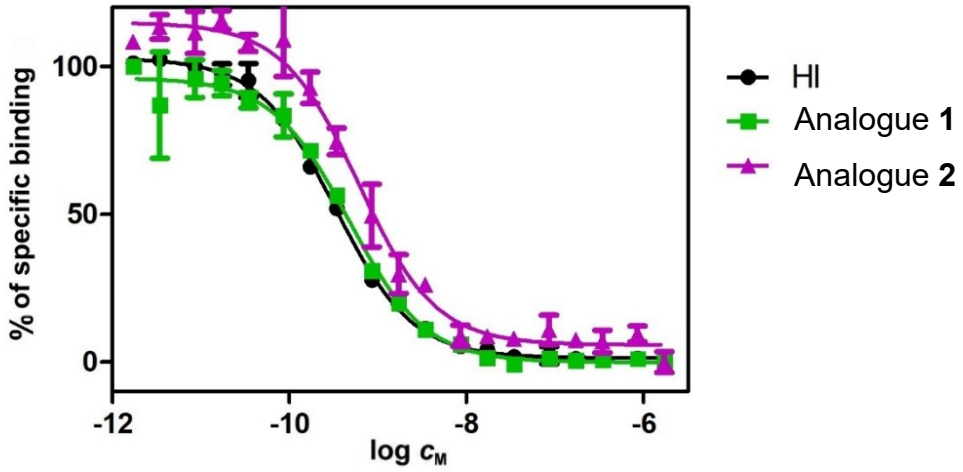

Figure 24. Inhibition of binding of human [^{125}I]-A14-insulin to human IR-A by human insulin (black), insulin analogue **1** (green) and insulin analogue **2** (pink). Representative curves for each analogue and human insulin are shown.

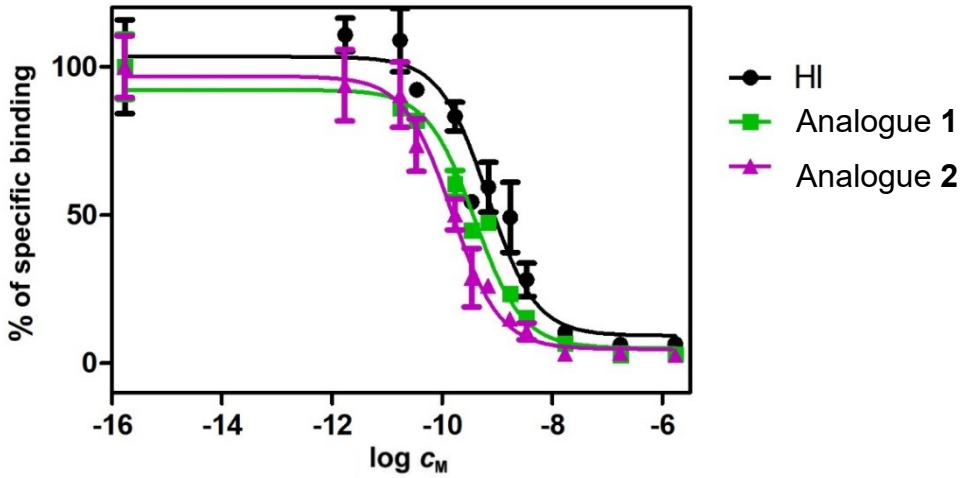

Figure 25. Inhibition of binding of human [^{125}I]-A14-insulin to human IR-B by human insulin (black), insulin analogue **1** (green) and insulin analogue **2** (pink). Representative curves for each of the analogue and human insulin are shown.

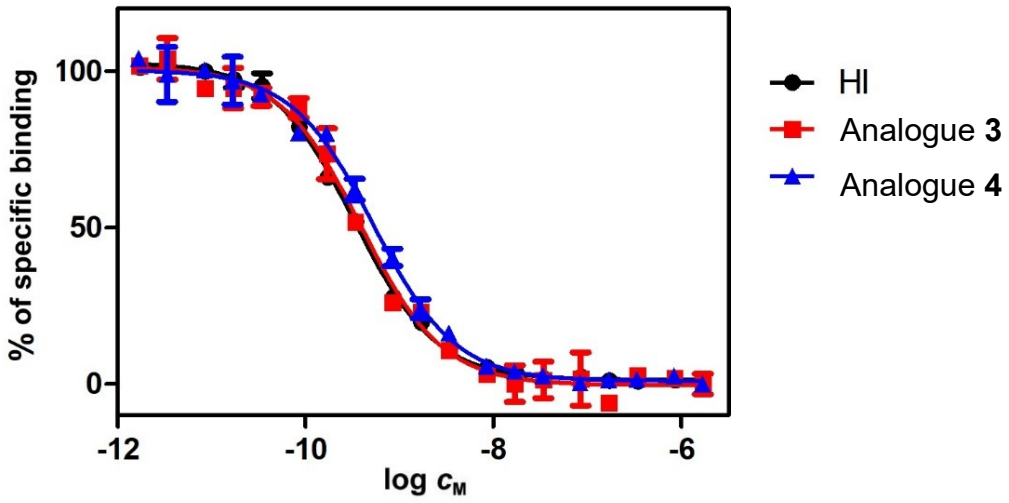

Figure 26. Inhibition of binding of human [^{125}I]-A14-insulin to human IR-A by human insulin (black), insulin analogue **3** (red) and insulin analogue **4** (blue). Representative curves for each of the analogues and human insulin are shown.

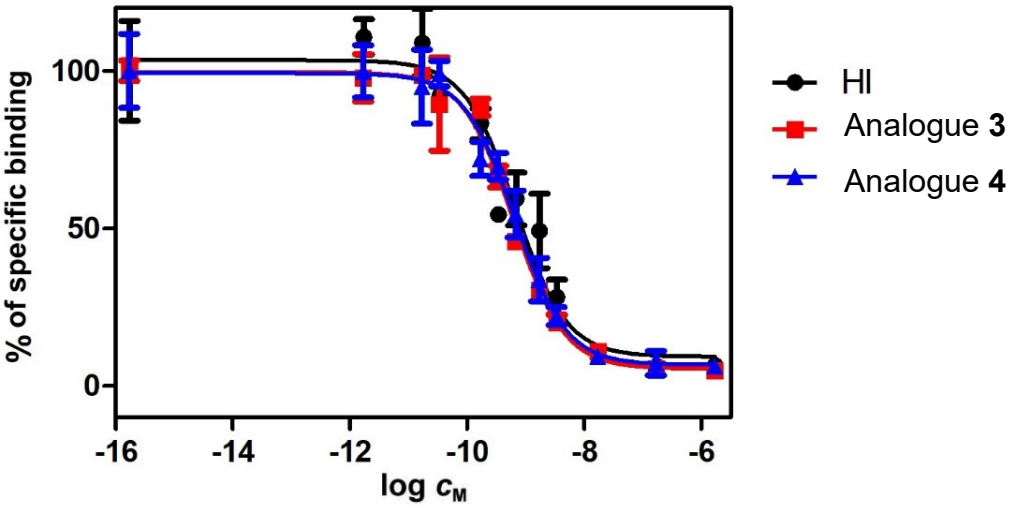

Figure 27. Inhibition of binding of human [^{125}I]-A14-insulin to human IR-B by human insulin (black), insulin analogue **3** (red) and insulin analogue **4** (blue). Representative curves for each of the analogues and human insulin are shown.

Table 8. The values of dissociation constants of analogues **1-4** for IR-A in membranes of human IM-9 lymphocytes and IR-B in membranes of transfected mouse fibroblasts and the relative binding affinities (%) of the analogues relative to human insulin binding affinity. The relative binding affinity is calculated according to the following formula: K_d (human insulin)/K_d (analogue) x 100 (%). The K_d values of analogues are related to K_d values of human insulin highlighted by the same colour. n is the number of binding curves from which the values were calculated. SEM is a standard error of mean.

Hormone	**K_d ± SEM (nM) for IR-A**	**Relative binding affinity [%]**	**K_d ± SEM (nM) for IR-B**	**Relative binding affinity [%]**	**Relative selectivity [%IR-B/%IR-A]**
Analogue **1** carboxymide(B30)-insulin	0.38 ± 0.04 (n=3)	152%	0.17 ± 0.09 (n=4)	206%	1.4
Analogue **2** GlyB31-carboxymide(B31)-insulin	0.53 ± 0.07 (n=3)	77%	0.19 ± 0.04 (n=3)	258%	3.4
Analogue **3** GlyB31-GlyB32-carboxymide(B32)-insulin	0.50 ± 0.17 (n=3)	82%	0.22 ± 0.09 (n=3)	223%	2.7
Analogue **4** GlyB31-GlyB32-GlyB33-carboxymide(B33)-insulin	0.65 ± 0.07 (n=3)	63%	0.79 ± 0.21 (n=3)	62%	1.0
HI	0.58 ± 0.08 (n=4) 0.41± 0.07 (n=4)	100% 100%	0.35 ± 0.04 (n=3) 0.49 ± 0.25 (n=3)	100% 100%	1.0

From the data shown in Table 8 (page 49), we can conclude that the relative binding affinities of analogues **1-3** were higher for IR-B than for IR-A. Therefore, these analogues are more IR-B specific than human insulin. The only exception is analogue **4**, which was equipotent to both isoforms of IR. The selectivity for IR-B was increased with the B-chain amidation (analogue **1**) and extension of the C-terminus for one or two Gly-amide (analogues **2** and **3**) but with the addition of three Gly-NH_2 (analogue **3**) the selectivity disappeared. The highest selectivity to IR-B was observed for analogue **2**, which has about 3.4-fold higher affinity to IR-B relative to IR-A. Almost all analogues (except for analogue **1** with 152%) had lower binding affinity for the isoform A of IR (about 60-80% of insulin). On the other hand, relative binding affinities of analogues **1-3** for IR-B were higher than affinity of human insulin in most cases (about 2-fold) and for analogue **2** even about 2.5-fold higher.

Next, we also determined binding affinities of analogues **2-4** for IGF-1R and compared them with binding affinity of human insulin [50] and human IGF-1. Testing for IGF-1R was done with R^{+39} cell line according to procedure described in chapter 4.6.5. The representative binding curves are shown in Figure 28 and the data are summarized in Table 9 (page 51).

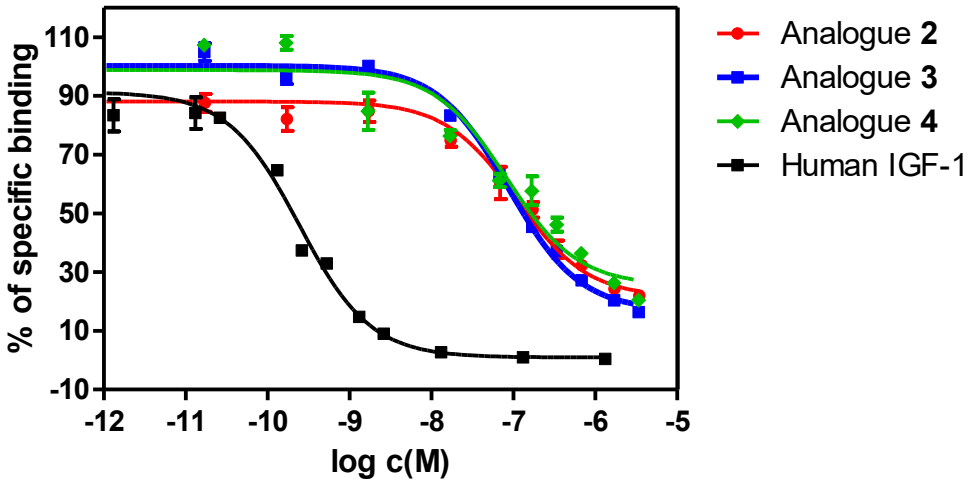

Figure 28. Inhibition of binding of human [^{125}I]-monoiodo-IGF-1 to human IGF-1R human IGF-1 (black), insulin analogue **2** (red), insulin analogue **3** (blue) and insulin analogue **4** (green). Representative curves for each of the analogues and human insulin are shown.

Table 9. The values of dissociation constants of analogues **2**-**4** for IGF-1R in membranes of transfected mouse fibroblasts and the relative binding affinities (%) of the analogues relative to human insulin binding affinity. The relative binding affinity is calculated according to the following formula: K_d (human IGF-1)/K_d (analogue) x 100 (%). n is the number of binding curves from which the values were determined. [a] In this case, the K_d value was calculated from three binding curves and has the character of the mean ± standard error. [b] In this case, the K_d value was calculated from two values and has the character of the mean ± range. [c] In this case, the K_d value was determined from only one binding curve. *From Vikova et al. (Ref. [50]). nd means not determined in this study.

Hormone	**K_d ± SEM (nM) for IGF-1R**	**Relative binding affinity [%]**
Analogue **1** carboxamide(B30)-insulin	nd	nd
Analogue **2** GlyB31-carboxamide(B31)-insulin	61 ± 25 (n=2)[b]	0.30%
Analogue **3** GlyB31-GlyB32-carboxamide(B32)-insulin	51 ± 7 (n=3)[a]	0.35%
Analogue **4** GlyB31-GlyB32-GlyB33-carboxamide(B33)-insulin	64 (n=1)[c]	0.28%
IGF-1	0.18 ± 0.03 (n=3)[a]	100%
Human insulin	nd	0.08%*

Relative binding affinities and K_d values of individual analogues to IGF-1R were similar. The analogue **4** had the highest K_d value of 64 nM and the analogue **3** exhibited the lowest K_d value of 51 nM. All analogues bind to IGF-1R significantly more strongly (about 3-4-times) than human insulin.

5.5. Abilities of the analogues to induce autophosphorylation of the receptors

In the last phase of experiments, the abilities of the analogues to induce phosphorylation of the receptor and specific cell signalling were determined. Activation of IR-A, IR-B and IGF-1R was measured in R−/IR-A, R−/IR-B, and R^{+39} cells, respectively. The individual receptors were activated by stimulation with different ligands by the method described in Chapter 4.7.3. The stimulation time was 10 minutes. Human insulin, IGF-1 and IGF-2 and all analogues were tested for IR-A and IR-B in two different concentrations, 10 nM and 1 nM. Phosphorylation of IGF-1R was tested with ligands only in 10 nM concentration. Primary and secondary antibodies are listed in Table 4 (page 35). The intensities of the resulting chemiluminescent signals characterizing the protein phosphorylation rate were detected and subsequently evaluated by the procedure described in Chapter 4.7.6. The resulting intensities were summarized in individual bar graphs (Figures 29-32, pages 53-55). Individual signal intensities are calculated relative to signal of insulin activation (for IR-A and IR-B) and IGF-1 activation signal (for IGF-1R).

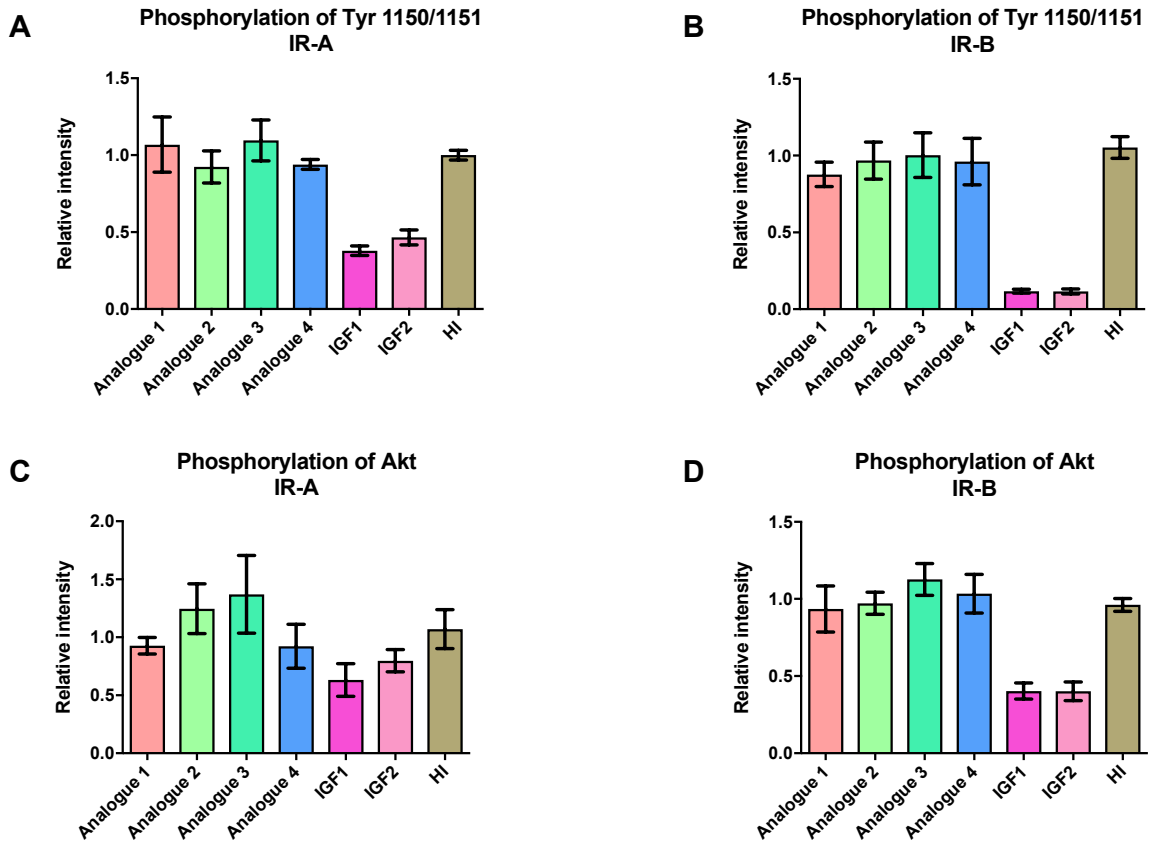

Figure 29. Relative abilities of analogues to activate individual receptors of human insulin (Figures 29A and B) and to phosphorylate Akt (Figure 29C and 29D) at 10 nM concentrations. On the left side is IR-A, on the right side is- IR-B. All intensities shown are calculated relative to signal of HI.

The results in Figure 29 show, that all four analogues stimulate IR-A autophosphorylation at 10 nM concentration similarly to HI (Figure 29A). The same results were found for IR-B (Figure 29B). Phosphorylation of Akt of IR isoforms follows similar trends shown by receptors' autophosphorylations (Figure 29CD).

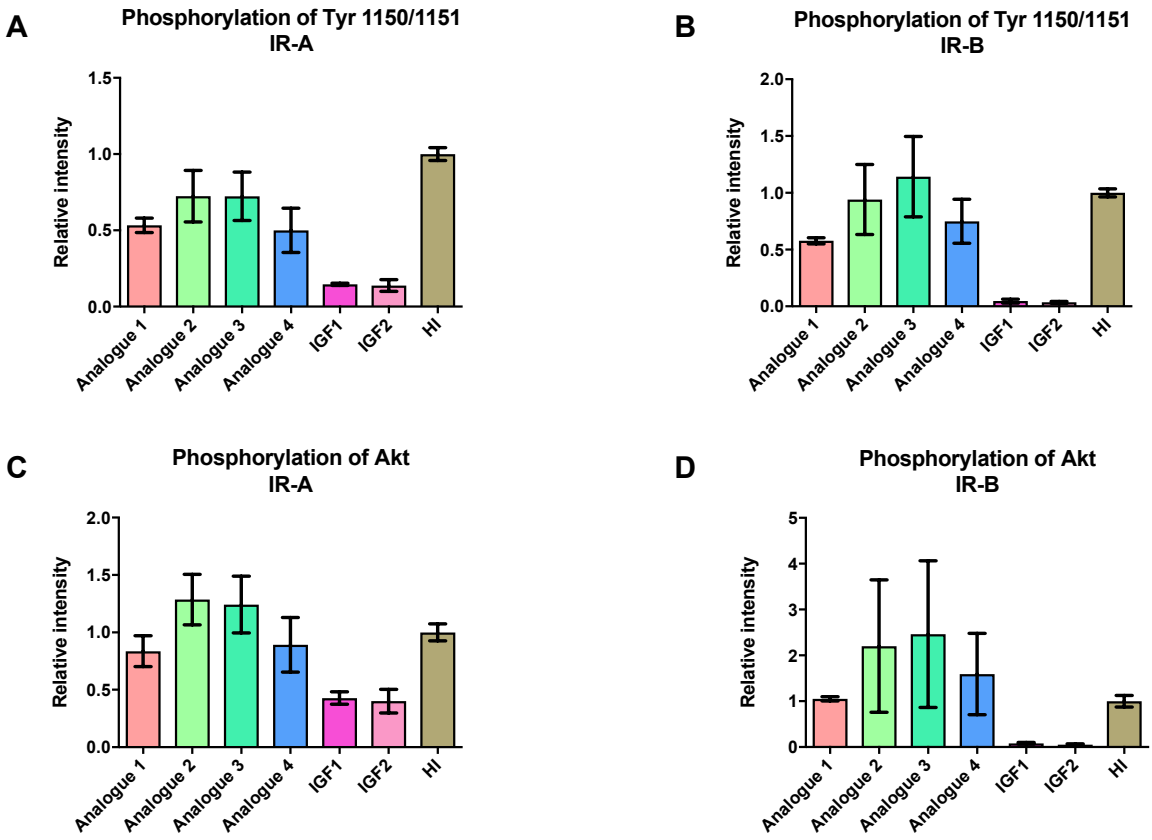

Figure 30. Relative abilities of analogues to activate insulin receptor isoforms (Figure 30A and B) and to phosphorylate Akt (Figure 30C and 30D) at 1 nM concentrations. On the left side is IR-A, on the right side is IR-B. All intensities are calculated relative to signal of HI.

In Figure 30, the relative abilities of ligands to activate IR and Akt at 1 nM concentration are shown. Here, we can see that the differences between analogues seem to be more visible than at 10 nM concentration and analogues **2** and **3** appear in IR-B stimulation slightly stronger than analogues **1** and **4** and possibly than human insulin as well. However, due to the overlap of experimental errors, the differences are rather showing trends than significant changes.

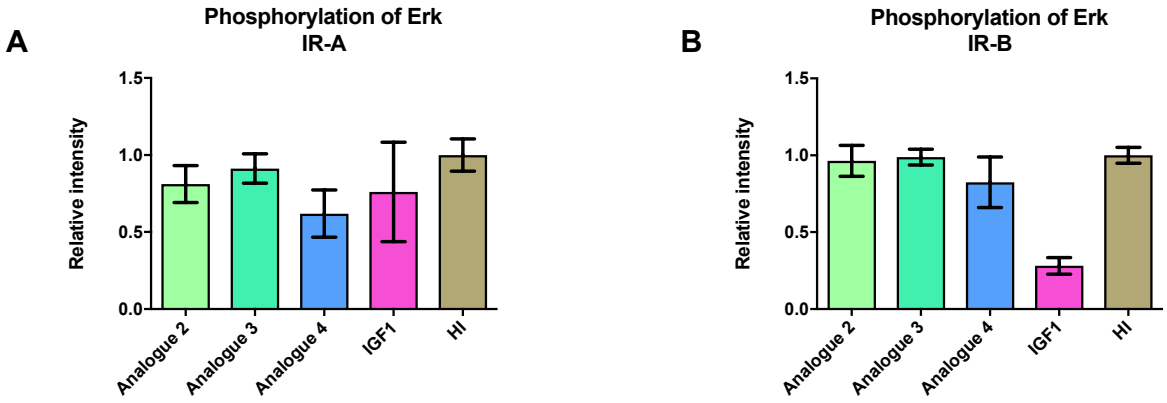

Figure 31. Relative abilities of analogues to phosphorylate Erk after induction of IR isoforms at 10 nM concentration. On the left side is IR-A, on the right side is IR-B. All intensities are calculated relative to signal of HI.

Next, phosphorylation of Erk (Figure 31) after the stimulation of IR-A and IR-B induced by 10 nM analogues was tested as well. The data showed that all analogues have similar ability to induce phosphorylation of Erk protein as native insulin. Analogue **1** was not tested due to the lack of time.

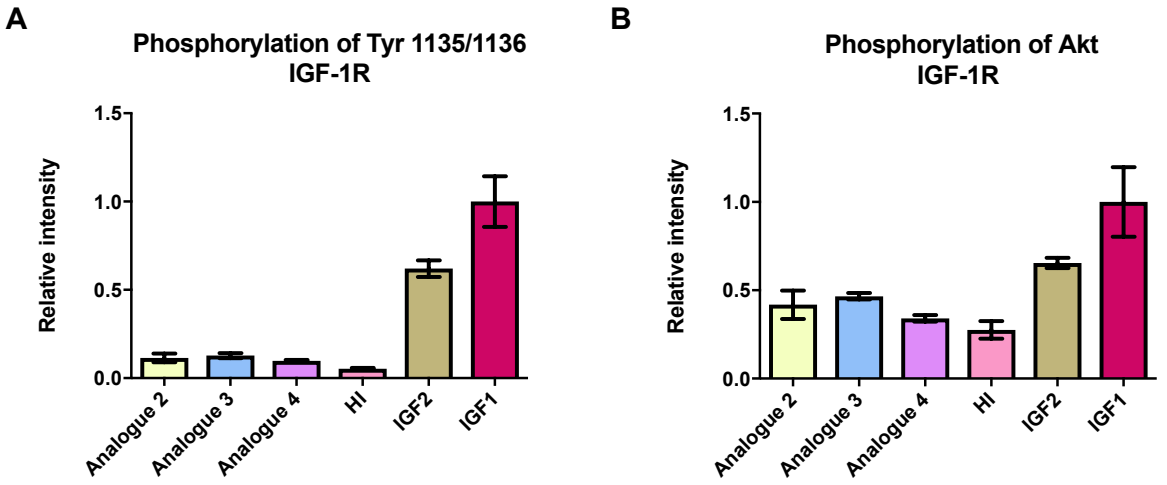

Figure 32. Relative abilities of analogues to activate autohphosphorylation of IGF-1R (Figure 31A) and phosphorylation of Akt after stimulation of IGF-1R (Figure 31B) at 10 nM concentration. All intensities are relative to signal of IGF-1R.

Finally, Figure 32 shows the abilities of analogues to activate receptor IGF-1R (Figure 31A) and Akt protein through receptor IGF-1R (Figure 31B) after stimulation at 10 nM concentration. Analogue **1** was not tested due to the lack of time.

In comparison to IGF-1 and IGF-2, the effect of stimulation by the analogues is significantly lower, especially in the activation of the receptor itself. Some trends may be visible indicating that especially the analogues **2** and **3** are stronger in activation of IGF-1R than human insulin.

Figure 33 shows the results of a routine experiment for controlling a uniform distribution of proteins in individual samples for stimulation experiments.

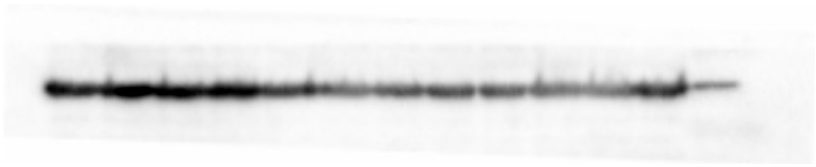

Figure 33. Control detection of total amount of protein using antibodies to Actin.

6. Discussion

In this work new insulin analogues with prolonged C-terminus of B-chain with Gly residues and amidated C-terminus were prepared. The plan of the study was to determine binding affinities of these analogues for IR-A, IR-B and, if possible, for IGF-1R and also to test abilities of analogues to induce autophosphorylation of IR-A and IR-B and subsequent signalling pathways. The purpose was to determine whether such analogues could be more selective for the IR-B isoform. The design of analogues was built on our previous observation [28] that the prolongation of the B-chain C-terminus can enhance binding and activation specificity of insulin for IR-B. Such analogues could find clinical applications in better maintaining glycaemia levels in diabetics (see in Introduction).

Here, we systematically prolonged the B-chain with 1-3 glycine residues. Glycine was selected because it lacks a side chain (and hence offers some uniformity in respect to other amino acids) and provides some degree of flexibility, which could be important for interaction with the receptor at this part of the binding site. Carboxyamidation of the C-terminus was used because it had positive effects on hormones shortened for B27-B30 [51][52].

The yields of individual analogues **1-4** were 5.5 mg, 1 mg, 1.7 mg and 0.3 mg, respectively. These results were influenced mainly by the yields of semisynthetic reactions and clearly demonstrate that one extra C-terminal residue in nonapeptide precursor is well tolerated by trypsin but that deca-, undeca- and mainly dodecapeptide are much poorer substrates for trypsin catalysed semisynthesis than shorter peptides. Therefore, semisynthesis by trypsin would not be an optimal method for a ligation of two larger peptide fragments. In agreement with that observation, lower yields of longer analogues (mainly **3** and **4**) were also obtained for the deprotection of Pac group by penicillin amidohydrolase (Table 7, page 46).

By testing the binding affinities for both receptor isoforms, we have found that all prepared analogues except analogue **4** bind more strongly to IR-B than to IR-A. Analogue **4** binds to both isoforms similarly to human insulin but with lower relative affinities. Analogues **1-3** were more / less selective for IR-B. Analogue **1** with a relative IR-B/IR-A selectivity of 1.4, analogue **2** with a relative selectivity of about 3.4, the highest of all prepared analogues. Analogue **3** binds IR-B isoform 2.7 times more strongly than IR-A compared to human insulin. All these findings are summarized in Figure 34 (page 58), where we can see the relationship between the prolongation of the C-terminus of B-chain and the

respective relative selectivity in comparison with HI. The prolongation of the C-terminus enhances IR-B specificity up to two extra glycines (analogues **2** and **3**) and a simple amidation has some minor positive effect as well (analogue **1**). The analogue **4** with 3 glycines already lacks any selectivity. Therefore, the extension of the C-terminus of the B-chain is likely to increase the affinity for IR-B only up to one or two extra C-amidated residues. It is possible that only two extra C-terminal amino acids can make some favourable contacts with α-CT peptide of IR-B. However, here, only the structural information about IR-B receptor could provide more answers. Anyhow, these results will be valuable for further design of IR-B selective analogues. On the other hand, we should not forget that these results should be considered only in the context of amino acid used (glycine) and amidated C-terminus. It is not ruled out that other amino acids could provide different results.

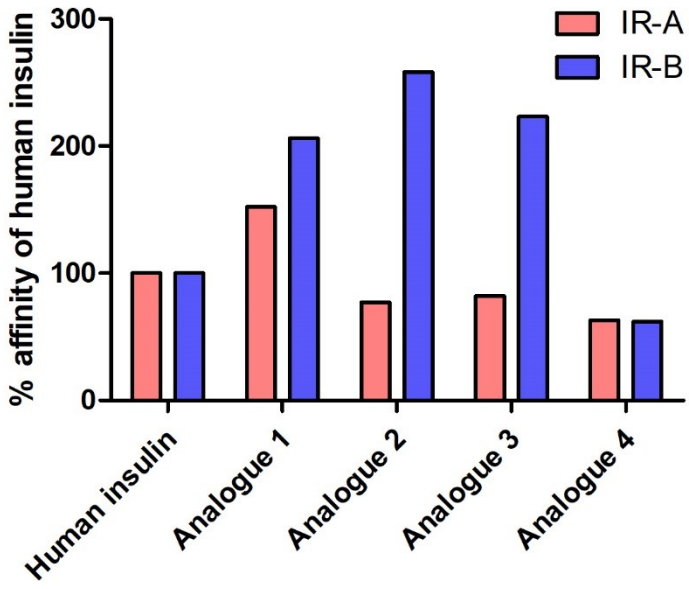

Figure 34. Ratio of relative binding affinities of analogues **1**-**4** for IR-A and IR-B. The values are relative (in %) to the binding affinity of human insulin (from Table 8, page 49).

The best method to determine the abilities of analogues to stimulate autophospohorylation of IR-A and IR-B is to measure their dose response curves [53]. However, this method is extremely laborious and time consuming especially when performing electrophoreses and western blotting as it was in our case. Therefore, in this study, we measured the abilities of analogues to activate receptors at 10 nM and 1 nM. In

the past we used this methodology to test the activities of a series of insulin [28] and IGF-1 analogues [54]. It provides a good method to reveal robust differences between analogues or major discrepancies between their affinities and activation capabilities, i.e. potential antagonism.

At 10 nM concentration, autophosporylation abilities as well as activations of Akt of individual analogues were very similar to insulin and there was no apparent difference between activation of IR-A and IR-B (Figure 29, page 53). On the other hand, when testing at 1 nM concentration, the abilities of analogues **2** and **3** to induce IR-B autophosphorylation seems to be slightly higher than the ability of native insulin and other analogues (Figure 30, page 54). This could mean that the receptors were over stimulated at 10 nM concentration and that testing of analogues at even lower concentration would be the best way. In future, for a publication of the results, we plan to determine dose response curves with IR-A and IR-B for at least analogues **2** and **3** and for human insulin in parallel.

7. Conclusion

We systematically investigated the effects of the prolongation of the C terminus of the B-chain of insulin for 1-3 glycine carboxamide residues on the receptor selectivity of resulting analogues. The addition of one or two glycines enhances the IR-B/IR-A binding specificity about 3-fold compared the human insulin. Addition of the three glycines has not a positive effect on IR-B/IR-A specificity. We also determined abilities of analogues to activate these receptors. It appears that the experiments at 10 or even 1 nM concentration of the analogues are not able to fully reveal differences between the analogues and that determination of dose response curves will be necessary to properly characterize their biological activities. In conclusion, this study fulfilled its aims and showed that the prolongation and amidation of the C-terminus of insulin can result in higher IR-B specificity of insulin. The data obtained in this study will be useful for the design of furthermore IR-B specific analogues, which could find applications in the treatment of diabetes.

8. References

[1] J. H. Jones, "A short guide to abbreviations and their use in peptide science," *Journal of Peptide Science*, vol. 5, no. 11, pp. 465–471, 1999.

[2] International Diabetes Federation (IDF), *IDF Diabetes Atlas 8th edition*. 2017.

[3] U. Derewenda, Z. Derewenda, G. G. Dodson, R. E. Hubbard, and F. Korber, "Molecular Structure of insulin: The insulin monomer and its assembly," *British Medical Bulletin*, vol. 45, no. 1, pp. 4–18, 1989.

[4] G. Bentley, E. Dodson, G. Dodson, D. Hodgkin, and D. Mercola, "Structure of insulin in 4-zinc insulin," *Nature*, vol. 261, no. 5556, pp. 166–168, 1976.

[5] E. A. Newsholme and G. Dimitriadis, "Integration of biochemical and physiologic effects of insulin on glucose metabolism," *Experimental and Clinical Endocrinology & Diabetes*, vol. 109, no. Suppl 2, pp. S122–S134, Nov. 2001.

[6] D. Ish-Shalom, C. T. Christoffersen, P. Vorwerk, N. Sacerdoti-Sierra, R. M. Shymko, D. Naor, and P. De Meyts, "Mitogenic properties of insulin and insulin analogues mediated by the insulin receptor," in *Diabetologia*, 1997, vol. 40, no. SUPPL. 2, pp. S25-31.

[7] P. De Meyts, "Insulin and its receptor: Structure, function and evolution," *BioEssays*, vol. 26, no. 12. pp. 1351–1362, 2004.

[8] Y. Fujita-Yamaguchi, T. R. LeBon, M. Tsubokawa, W. Henzel, S. Kathuria, D. Koyal, and J. Ramachandran, "Comparison of insulin-like growth factor I receptor and insulin receptor purified from human placental membranes.," *The Journal of biological chemistry*, vol. 261, no. 35, pp. 16727–31, Dec. 1986.

[9] T. E. Adams, V. C. Epa, T. P. Garrett, and C. W. Ward, "Structure and function of the type 1 insulin-like growth factor receptor.," *Cellular and molecular life sciences : CMLS*, vol. 57, no. 7, pp. 1050–93, 2000.

[10] P. De Meyts, "The insulin receptor: a prototype for dimeric, allosteric membrane receptors?," *Trends in Biochemical Sciences*, vol. 33, no. 8. pp. 376–384, Aug-2008.

[11] A. Ullrich, A. Gray, A. W. Tam, T. Yang-Feng, M. Tsubokawa, C. Collins, W. Henzel, T. Le Bon, S. Kathuria, and E. Chen, "Insulin-like growth factor I receptor primary structure: comparison with insulin receptor suggests structural determinants that define functional specificity.," *The EMBO Journal*, vol. 5, no. 10, pp. 2503–12, 1986.

[12] M. C. Lawrence, N. M. Mckern, and C. W. Ward, “Insulin receptor structure and its implications for the IGF-1 receptor,” *Current Opinion in Structural Biology*, vol. 17, pp. 699–705, 2007.

[13] T. I. Croll, B. J. Smith, M. B. Margetts, J. Whittaker, M. A. Weiss, C. W. Ward, and M. C. Lawrence, “Higher-Resolution Structure of the Human Insulin Receptor Ectodomain: Multi-Modal Inclusion of the Insert Domain,” *Structure*, vol. 24, no. 3, pp. 469–476, 2016.

[14] S. Seino, M. Seino, S. Nishi, and G. I. Bell, “Structure of the human insulin receptor gene and characterization of its promoter.,” *Proceedings of the National Academy of Sciences of the United States of America*, vol. 86, no. 1, pp. 114–118, 1989.

[15] F. Westermeier, T. Sáez, P. Arroyo, F. Toledo, J. Gutiérrez, C. Sanhueza, F. Pardo, A. Leiva, and L. Sobrevia, “Insulin receptor isoforms: An integrated view focused on gestational diabetes mellitus,” *Diabetes/Metabolism Research and Reviews*, vol. 32, no. 4. pp. 350–365, 2016.

[16] A. Belfiore, R. Malaguarnera, V. Vella, M. C. Lawrence, L. Sciacca, F. Frasca, A. Morrione, and R. Vigneri, “Insulin receptor isoforms in physiology and disease: An updated view,” *Endocrine Reviews*, vol. 38, no. 5, pp. 1–84, 2017.

[17] M. A. Soos and K. Siddle, “Immunological relationships between receptors for insulin and insulin-like growth factor I. Evidence for structural heterogeneity of insulin-like growth factor I receptors involving hybrids with insulin receptors,” *Biochem J*, vol. 263, no. 2, pp. 553–563, 1989.

[18] E. M. Bailyes, B. T. Navé, M. A. Soos, S. R. Orr, A. C. Hayward, and K. Siddle, “Insulin receptor/IGF-I receptor hybrids are widely distributed in mammalian tissues: quantification of individual receptor species by selective immunoprecipitation and immunoblotting.,” *The Biochemical journal*, vol. 327 (Pt 1, pp. 209–15, 1997.

[19] P. De Meyts, “Insulin/receptor binding: The last piece of the puzzle?: What recent progress on the structure of the insulin/ receptor complex tells us (or not) about negative cooperativity and activation P. D. Meyts,” *BioEssays*, vol. 37, no. 4, pp. 389–397, Apr. 2015.

[20] P. De Meyts, E. Van Obberghen, J. Roth, A. Wollmer, and D. Brandenburg, “Mapping of the residues responsible for the negative cooperativity of the receptor-binding region of insulin,” *Nature*, vol. 273, no. 5663, pp. 504–509, 1978.

[21] L. Gauguin, C. Delaine, C. L. Alvino, K. A. McNeil, J. C. Wallace, B. E. Forbes, and P. De Meyts, "Alanine scanning of a putative receptor binding surface of insulin-like growth factor-I," *Journal of Biological Chemistry*, vol. 283, no. 30, pp. 20821–20829, Jul. 2008.

[22] P. F. Williams, D. C. Mynarcik, Gui Qin Yu, and J. Whittaker, "Mapping of an NH2-terminal ligand binding site of the insulin receptor by alanine scanning mutagenesis," *Journal of Biological Chemistry*, vol. 270, no. 7, pp. 3012–3016, 1995.

[23] J. G. Menting, J. Whittaker, M. B. Margetts, L. J. Whittaker, G. K. W. Kong, B. J. Smith, C. J. Watson, L. Žáková, E. Kletvíková, J. Jiráček, S. J. Chan, D. F. Steiner, G. G. Dodson, A. M. Brzozowski, M. A. Weiss, C. W. Ward, and M. C. Lawrence, "How insulin engages its primary binding site on the insulin receptor," *Nature*, vol. 493, no. 7431, pp. 241–245, 2013.

[24] J. G. Menting, Y. Yang, S. J. Chan, N. B. Phillips, B. J. Smith, J. Whittaker, N. P. Wickramasinghe, L. J. Whittaker, V. Pandyarajan, Z. -l. Wan, S. P. Yadav, J. M. Carroll, N. Strokes, C. T. Roberts, F. Ismail-Beigi, W. Milewski, D. F. Steiner, V. S. Chauhan, C. W. Ward, M. A. Weiss, and M. C. Lawrence, "Protective hinge in insulin opens to enable its receptor engagement," *Proceedings of the National Academy of Sciences*, vol. 111, no. 33, pp. E3395–E3404, 2014.

[25] L. Whittaker, C. Hao, W. Fu, and J. Whittaker, "High-affinity insulin binding: Insulin interacts with two receptor ligand binding sites," *Biochemistry*, vol. 47, no. 48, pp. 12900–12909, 2008.

[26] G. Scapin, V. P. Dandey, Z. Zhang, W. Prosise, A. Hruza, T. Kelly, T. Mayhood, C. Strickland, C. S. Potter, and B. Carragher, "Structure of the Insulin Receptor–Insulin Complex by Single Particle CryoEM analysis," *Nature*, vol. 556, no. 7699, pp. 122–125, Feb. 2018.

[27] J. Jiráček and L. Žáková, "Structural perspectives of insulin receptor isoform-selective insulin analogs," *Frontiers in Endocrinology*, vol. 8, no. JUL, 2017.

[28] K. Křížková, M. Chrudinová, A. Povalová, I. Selicharová, M. Collinsová, V. Vaněk, A. M. Brzozowski, J. Jiráček, and L. Zakova, "Insulin-Insulin-like Growth Factors Hybrids as Molecular Probes of Hormone:Receptor Binding Specificity," *Biochemistry*, vol. 55, no. 21, pp. 2903–2913, 2016.

[29] V. V. Kiselyov, S. Versteyhe, L. Gauguin, and P. De Meyts, “Harmonic oscillator model of the insulin and IGF1 receptors’ allosteric binding and activation,” *Molecular Systems Biology*, vol. 5, 2009.

[30] T. Gutmann, K. H. Kim, M. Grzybek, T. Walz, and Ü. Coskun, “Visualization of ligand-induced transmembrane signaling in the full-length human insulin receptor.,” *The Journal of cell biology*, p. jcb.201711047, 2018.

[31] J. Avruch, “Insulin signal transduction through protein kinase cascades.,” *Molecular and cellular biochemistry*, vol. 182, no. 1–2, pp. 31–48, 1998.

[32] C. M. Taniguchi, B. Emanuelli, and C. R. Kahn, “Critical nodes in signalling pathways: Insights into insulin action,” *Nature Reviews Molecular Cell Biology*, vol. 7, no. 2. pp. 85–96, 2006.

[33] D. R. Alessi, S. R. James, C. P. Downes, A. B. Holmes, P. R. J. Gaffney, C. B. Reese, and P. Cohen, “Characterization of a 3-phosphoinositide-dependent protein kinase which phosphorylates and activates protein kinase Bα,” *Current Biology*, vol. 7, no. 4, pp. 261–269, Apr. 1997.

[34] H. Sano, “Insulin-stimulated Phosphorylation of a Rab GTPase-activating Protein Regulates GLUT4 Translocation,” *Journal of Biological Chemistry*, vol. 278, no. 17, pp. 14599–14602, 2003.

[35] C. P. Mîinea, H. Sano, S. Kane, E. Sano, M. Fukuda, J. Peränen, W. S. Lane, and G. E. Lienhard, “AS160, the Akt substrate regulating GLUT4 translocation, has a functional Rab GTPase-activating protein domain,” *Biochemical Journal*, vol. 391, no. 1, pp. 87–93, Oct. 2005.

[36] S. Frame and P. Cohen, “GSK3 takes centre stage more than 20 years after its discovery.,” *The Biochemical journal*, vol. 359, no. Pt 1, pp. 1–16, 2001.

[37] P. Puigserver, J. Rhee, J. Donovan, C. J. Walkey, J. C. Yoon, F. Oriente, Y. Kitamura, J. Altomonte, H. Dong, D. Accili, and B. M. Spiegelman, “Insulin-regulated hepatic gluconeogenesis through FOXO1-PGC-1α interaction,” *Nature*, vol. 423, no. 6939, pp. 550–555, 2003.

[38] P. R. Shepherd, D. J. Withers, and K. Siddle, “Phosphoinositide 3-kinase : the key switch mechanism in insulin signalling,” *Biochem. J*, vol. 333, no. Pt 3, pp. 471–490, Aug. 1998.

[39] T. Sasaoka and M. Kobayashi, “The Functional Significance of Shc in Insulin Signaling as a Substrate of the Insulin Receptor,” *Endocrine Journal*, vol. 47, no. 4, pp. 373–381, 2000.

[40] J. Pouysségur, V. Volmat, and P. Lenormand, “Fidelity and spatio-temporal control in MAP kinase (ERKs) signalling,” *Biochemical Pharmacology*, vol. 64, no. 5–6, pp. 755–763, 2002.

[41] G. L. Johnson and R. Lapadat, “Mitogen-activated protein kinase pathways mediated by ERK, JNK, and p38 protein kinases,” *Science*, vol. 298, no. 5600. pp. 1911–1912, 2002.

[42] R. Chandra and R. A. Liddle, “Recent advances in the regulation of pancreatic secretion,” *Current Opinion in Gastroenterology*, vol. 30, no. 5. pp. 490–494, 2014.

[43] M. Komatsu, M. Takei, H. Ishii, and Y. Sato, “Glucose-stimulated insulin secretion: A newer perspective,” *Journal of Diabetes Investigation*, vol. 4, no. 6. pp. 511–516, 2013.

[44] R. Herring, R. H. Jones, and D. L. Russell-Jones, “Hepatoselectivity and the evolution of insulin,” *Diabetes, Obesity and Metabolism*, vol. 16, no. 1. pp. 1–8, 2014.

[45] A. L. Olson and J. E. Pessin, “Structure, function, and regulation of the mammalian facilitative glucose transporter gene family,” *Annu Rev Nutr*, vol. 16, pp. 235–256, 1996.

[46] D. S. Edgerton, M. Lautz, M. Scott, C. A. Everett, K. M. Stettler, D. W. Neal, C. A. Chu, and A. D. Cherrington, “Insulin’s direct effects on the liver dominate the control of hepatic glucose production,” *Journal of Clinical Investigation*, vol. 116, no. 2, pp. 521–527, 2006.

[47] S. V. M. Hordern, J. E. Wright, A. M. Umpleby, F. Shojaee-Moradie, J. Amiss, and D. L. Russell-Jones, “Comparison of the effects on glucose and lipid metabolism of equipotent doses of insulin detemir and NPH insulin with a 16-h euglycaemic clamp,” *Diabetologia*, vol. 48, no. 3, pp. 420–426, 2005.

[48] S. G. Vienberg, S. D. Bouman, H. Sørensen, C. E. Stidsen, T. Kjeldsen, T. Glendorf, A. R. Sørensen, G. S. Olsen, B. Andersen, and E. Nishimura, “Receptor-isoform-selective insulin analogues give tissue-preferential effects,” *Biochemical Journal*, vol. 440, no. 3, pp. 301–308, 2011.

[49] L. Žáková, D. Zyka, J. Ježek, I. Hančlová, M. Šanda, A. M. Brzozowski, and J. Jiráček, “The use of Fmoc-Lys(Pac)-OH and penicillin G acylase in the preparation of novel semisynthetic insulin analogs,” *Journal of Peptide Science*, vol. 13, no. 5, pp. 334–341, May 2007.

[50] J. Viková, M. Collinsová, E. Kletvíková, M. Buděšínský, V. Kaplan, L. Žáková, V. Veverka, R. Hexnerová, R. J. T. Aviñó, J. Straková, I. Selicharová, V. Vaněk, D. W. Wright, C. J. Watson, J. P. Turkenburg, A. M. Brzozowski, and J. Jiráček, “Rational steering of insulin binding specificity by intra-chain chemical crosslinking,” *Scientific Reports*, vol. 6, p. 19431, 2016.

[51] L. Žáková, L. Kazdová, I. Hančlová, E. Protivínská, M. Šanda, M. Buděšínský, and J. Jiráček, “Insulin analogues with modifications at position B26. Divergence of binding affinity and biological activity,” *Biochemistry*, vol. 47, no. 21, pp. 5858–5868, May 2008.

[52] L. Žáková, T. Barth, J. Jiráček, J. Barthová, and Š. Zórad, “Shortened Insulin Analogues: Marked Changes in Biological Activity Resulting from Replacement of TyrB26 and N-Methylation of Peptide Bonds in the C-Terminus of the B-Chain,” *Biochemistry*, vol. 43, no. 8, pp. 2323–2331, Mar. 2004.

[53] K. Macháčková, M. Chrudinová, J. Radosavljević, P. Potalitsyn, K. Křížková, M. Fábry, I. Selicharová, M. Collinsová, A. M. Brzozowski, L. Žáková, and J. Jiráček, “Converting Insulin-like Growth Factors 1 and 2 into High-Affinity Ligands for Insulin Receptor Isoform A by the Introduction of an Evolutionarily Divergent Mutation,” *Biochemistry*, p. acs.biochem.7b01260, Apr. 2018.

[54] K. Macháčková, M. Collinsová, M. Chrudinová, I. Selicharová, J. Pícha, M. Buděšínský, V. Vaněk, L. Žáková, A. M. Brzozowski, and J. Jiráček, “Insulin-like Growth Factor 1 Analogs Clicked in the C Domain: Chemical Synthesis and Biological Activities,” *Journal of Medicinal Chemistry*, vol. 60, no. 24, pp. 10105–10117, Dec. 2017.